*Nucleic Acids Research*, 2025, **53**, gkae735
https://doi.org/10.1093/nar/gkae735
Advance access publication date: 4 September 2024
**RNA and RNA-protein complexes**

# Mechanism of activation of contact-dependent growth inhibition tRNase toxin by the amino acid biogenesis factor CysK in the bacterial competition system

**Zhaohang Feng, Yuka Yashiro and Kozo Tomita***

Department of Computational Biology and Medical Sciences, Graduate School of Frontier Sciences, The University of Tokyo, Kashiwa, Chiba 277-8562, Japan

*To whom correspondence should be addressed. Tel: +81 471363611; Fax: +81 471363611; Email: kozo-tomita@edu.k.u-tokyo.ac.jp

## Abstract

Contact-dependent growth inhibition (CDI) is a bacterial competition mechanism, wherein the C-terminal toxin domain of CdiA protein (CdiA-CT) is transferred from one bacterium to another, impeding the growth of the toxin recipient. In uropathogenic *Escherichia coli* 536, CdiA-CT (CdiA-CT$^{EC536}$) is a tRNA anticodon endonuclease that requires a cysteine biogenesis factor, CysK, for its activity. However, the mechanism underlying tRNA recognition and cleavage by CdiA-CT$^{EC536}$ remains unresolved. Here, we present the cryo-EM structure of the CysK:CdiA-CT$^{EC536}$:tRNA ternary complex. The interaction between CdiA-CT$^{EC536}$ and CysK stabilizes the CdiA-CT$^{EC536}$ structure and facilitates tRNA binding and the formation of the CdiA-CT$^{EC536}$ catalytic core structure. The bottom-half of the tRNA interacts exclusively with CdiA-CT$^{EC536}$ and the $\alpha$-helices of CdiA-CT$^{EC536}$ engage with the minor and major grooves of the bottom-half of tRNA, positioning the tRNA anticodon loop at the CdiA-CT$^{EC536}$ catalytic site for tRNA cleavage. Thus, CysK serves as a platform facilitating the recognition and cleavage of substrate tRNAs by CdiA-CT$^{EC536}$.

## Graphical abstract

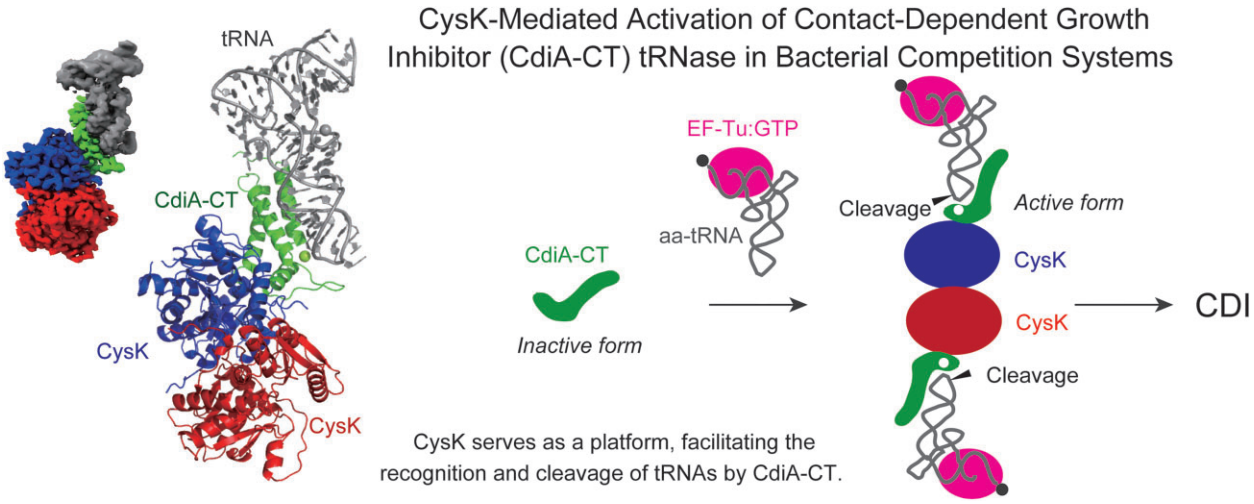


## Introduction

Contact-dependent growth inhibition (CDI) is a bacterial competition mechanism widely observed in Gram-negative bacteria, and particularly in pathogenic proteobacteria (1–5). CDI proceeds through direct cell-to-cell contact between closely related bacteria, followed by transfer of toxic proteins from one bacterium to another. The toxin protein transfer leads to the growth inhibition of the neighboring bacterium that received the toxin protein. The genes of the CDI system are *cdiB*, *cdiA* and *cdiI*, forming the *cdiBAI* gene cluster (1). CdiB is an outer membrane protein that facilitates the secretion of the CdiA exoprotein. After CdiA binding to specific receptors on the surfaces of neighboring bacteria, the C-terminal toxin domain of CdiA (CdiA-CT) is cleaved from CdiA, and CdiA-CT translocates into them (4,6–8). CdiI is an immunity protein that neutralizes the toxicity of CdiA-CT. Thus, CdiA-CT inhibits the growth of non-isogenic neighboring bacteria that lack the cognate *cdiI* gene and do not express CdiI.

**Received:** July 2, 2024. **Revised:** August 9, 2024. **Editorial Decision:** August 11, 2024. **Accepted:** August 14, 2024

Isogenic bacteria that have the same *cdiB*, *cdiA* and *cdiI* gene cluster express a cognate CdiI against the CdiA-CT, thereby preventing self-intoxication/inhibition (9,10).

The modes of action of CdiA-CTs are polymorphic, and include DNase, RNase, and pore-forming activities that suppress bacterial growth (2). CdiA-CTs with RNase activity target rRNA and tRNA in cells and inhibit protein synthesis. Some CdiA-CTs are tRNases that cleave the acceptor stem of tRNAs, while others cleave the anticodon loop of tRNAs (11). Although some CdiA-CTs exhibit intrinsic tRNase activity, others require an additional factor(s) for their tRNase activities (12–18). The CdiA-CTs in enterohemorrhagic *Escherichia coli* EC869, NC101, and *Klebsiella pneumoniae*, which cleave the 3′ acceptor regions of tRNAs, require the translation elongation factors EF-Tu, EF-Ts, and GTP for their activities (16–19). The CdiA-CT from EC869 (CdiA-CT$^{EC869}$) reportedly forms a quaternary complex with Tu:GTP:Ts, which increases the affinity of CdiA-CT$^{EC869}$ for substrate tRNAs and induces structural changes in them for efficient cleavage by CdiA-CT$^{EC869}$ (20). Thus, the Tu:GTP:Ts complex could serve as a reaction scaffold for tRNA cleavage by CdiA-CTs, beyond its established function in protein synthesis. In uropathogenic *E. coli* EC536, CdiA-CT (CdiA-CT$^{EC536}$), which cleaves the tRNA anticodon loop, requires the cysteine biogenesis factor *O*-acetylserine sulfhydrylase A (CysK) for its activity, and CdiA-CT$^{EC536}$ interacts with CysK (12,14,15). The canonical function of CysK is to synthesize cysteine from *O*-acetylserine and hydrogen sulfide. The interaction between CdiA-CT$^{EC536}$ and CysK may stabilize the interaction between CdiA-CT$^{EC536}$ and CdiI$^{EC536}$ (14). In addition, the CysK:CdiA-CT$^{EC536}$ interaction may reinforce the CdiA-CT$^{EC536}$ structure and increase the affinity of the complex for the tRNA substrate (13). However, the precise mechanism underlying the recognition and cleavage of tRNAs by the CysK:CdiA-CT$^{EC536}$ complex remains unresolved.

Here, we present the cryo-EM structure of the CysK:CdiA-CT$^{EC536}$:tRNA ternary complex. The structure revealed that CysK serves as a platform that facilitates the recognition and cleavage of substrate tRNAs by CdiA-CT$^{EC536}$ in the CDI bacterial competition system.

## Materials and methods

### Plasmid construction

Synthetic DNAs encoding the *cdi*A-CT- *cdi*I module from uropathogenic *Escherichia coli* 536 (*cdi*A-CT$^{EC536}$-*cdi*I, accession number WP_000554175.1) and the catalytically inactive *cdi*A-CT (*cdi*A-CT$^{EC536}$_H178A) were purchased from Eurofins, Japan. The nucleotide sequences of *cdi*A-CT$^{EC536}$-*cdi*I and *cdi*A-CT$^{EC536}$_H178A are provided in Supplementary Table 1. For cysteine synthase A (CysK, accession number WP_000 034 402) overexpression in *E. coli,* the *cysK* gene was PCR amplified from *E. coli* MG1655 (NIG, Japan) genomic DNA and cloned between the *Nde*I and *Xho*I sites of pET22b (Novagen-Merck Millipore), yielding pET22-CysK. To generate plasmids for the expression of the catalytically inactive CdiA-CT$^{EC536}$_H178A mutant protein, synthetic DNA encoding *cdi*A-CT$^{EC536}$_H178A was PCR amplified and cloned between the *Nde*I and *Xho*I sites of pET22b (Novagen-Merck Millipore), yielding the plasmid pET22-CdiA-CT$^{EC536}$_H178A. pET22-CdiA-CT$^{EC536}$ variants with deletions of the C-terminal region of the CdiA-CT$^{EC536}$ coding region were prepared by PCR. For co-expression of CdiA-CT$^{EC536}$ and CdiI, the *cdi*A-CT$^{EC536}$-*cdi*I module was cloned between the *Nde*I and *Xho*I sites of pET22b (Novagen-Merck Millipore), yielding pET22-CdiA-CT$^{EC536}$-CdiI. For co-expression of CysK and CdiA-CT$^{EC536}$_H178A, the *cysK* gene was PCR amplified and first cloned between the *Nco*I and EcoRI sites of pETDuet-1 (Novagen-Merck Millipore), yielding pETDuet-CysK. Then, *cdi*A-CT$^{EC536}$_H178A was cloned between the *Nde*I and *Xho*I sites of pETDuet-CysK, yielding the plasmid pETDuet-CysK-CdiA-CT$^{EC536}$_H178A. The DNA fragment encoding CdiA-CT$^{EC536}$ lacking the terminal Ile227, CdiA-CT$^{EC536}$_ΔI227, was PCR amplified and cloned between the *Nde*I and *Hin*dIII sites of the modified pBAD33.1 vector (ATCC87402) (20), yielding pBAD_CdiA-CT$^{EC536}$_ΔI227. Wild-type CdiA-CT$^{EC536}$ cloned into modified pBAD33.1 was not obtained, due to the toxicity of CdiA-CT$^{EC536}$. Thus, CdiA-CT$^{EC536}$_ΔI227 was used as the 'wild-type' and the relative toxicities of CdiA-CT$^{EC536}$ variants to the 'wild-type' were evaluated in this study (Figure 3 and Figure 5). pBAD33_CdiA-CT$^{EC536}$ variants with a mutation in the *Cdi*A-CT$^{EC536}$ coding region were prepared by PCR, using pBAD_CdiA-CT$^{EC536}$_ΔI227 as the template. The oligonucleotide primers used for the PCR cloning and mutations are listed in Supplementary Table 2.

### Protein expression and purification

For the expression of the CysK:CdiA-CT(H178A) complex and the CdiA-CT:CdiI complex, *E. coli* BL21(DE3) (Novagen-Merck Millipore) was transformed with pETDuet-CysK-CdiA-CT$^{EC536}$_H178A and pET22-CdiA-CT$^{EC536}$-CdiI, respectively, and cultures were incubated until the $OD_{660}$ reached 0.8. Protein expression was induced by the addition of 0.1 mM isopropyl-β-D-thiogalactopyranoside (IPTG), and the culture was continued for 16 hours at 20°C. For the expression of CysK and CdiA-CT(H178A), *E. coli* BL21(DE3) and Rosetta (DE3) (Novagen-Merck Millipore) were transformed with pET22-CysK and pET15-CdiA-CT$^{EC536}$_H178A, respectively. Protein expression was induced as described above.

The harvested cells, expressing CysK:CdiA-CT(H178A), CdiA-CT:CdiI, CysK or CdiA-CT(H178A), were lysed in buffer A (50 mM Tris–Cl, pH 7.0, 500 mM NaCl, 10% (v/v) glycerol, 20 mM imidazole, and 5 mM β-mercaptoethanol) supplemented with 0.1 mM PMSF (phenylmethylsulfonyl fluoride) and 50 μg/mL lysozyme. The lysates were cleared by centrifugation at 30 000 × g and 4°C for 45 min, and the supernatants were applied to a Ni-NTA column (QIAGEN, Japan). The column was washed with buffer A, and the proteins were eluted with buffer B (50 mM Tris–Cl, pH 7.0, 500 mM NaCl, 10% (v/v) glycerol, 500 mM imidazole, 5 mM β-mercaptoethanol). The proteins were then applied to a Hi-Trap Heparin (or Hi-Trap Q) column (GE Healthcare, Japan). Finally, the proteins were purified on a Hi-Load 16/60 Superdex 200 column (GE Healthcare, Japan), equilibrated with buffer containing 25 mM Tris–Cl, pH 7.0, 150 mM NaCl, and 10 mM β-mercaptoethanol, and concentrated.

For the purification of wild-type CdiA-CT, we used the CdiA-CT:CdiI complex partially purified on the Hi-Trap Q column after the Ni-NTA column, as described. The fractions containing CdiA-CT and CdiI were pooled, and the proteins were loaded onto the Ni-NTA column. After washing the column with buffer A, the column was washed with buffer containing 20 mM Tris–Cl, pH 8.0, 500 mM NaCl and 8 M urea,

and wild-type CdiA-CT was separated from CdiI and eluted from the column. Subsequently, wild-type CdiA-CT was dialyzed against buffer containing 20 mM Tris–Cl, pH 7.0, 85 mM NaCl and 10 mM β-mercaptoethanol. Finally, wild-type CdiA-CT was purified on a Hi-Load 16/60 Superdex 200 column. The CdiI protein partially purified on the Hi-TrapQ column, as described above, was further purified on a Hi-Load 16/60 Superdex 200 column.

## tRNA preparation

*E. coli* $tRNA^{Ile}GAU$ was overexpressed in *E. coli* using the pBSTNAV3 plasmid encoding the $tRNA^{Ile}GAU$ (Accession number: NC_000913.3) precursor gene, and purified as described (21–23). The *E. coli* JM101Tr strain was transformed with the pBSTNAV3 plasmid (24,25) containing the $tRNA^{Ile}GAU$ precursor gene and cultured in 2× YT medium containing 50 μg/ml ampicillin at 37°C for at least 24 h. Total RNAs were prepared as described (26), and then loaded on a HiLoad 16/10 Q-Sepharose HP column (GE Healthcare, Japan) and separated by a linear NaCl gradient (0.2–1.0 M) in buffer containing 20 mM Tris–Cl, pH 7.4, 0.1 mM EDTA and 8 mM $Mg(OAc)_2$. The fractions enriched with the overexpressed $tRNA^{Ile}GAU$ were detected by an aminoacylation assay, using the cognate aminoacyl-tRNA synthetases. The fractions containing overexpressed $tRNA^{Ile}GAU$ were further separated on a reverse phase DELTA-PAK C4 column (Waters, Japan), and the tRNA was detected by aminoacylation. The $tRNA^{Ile}GAU$ was ethanol-precipitated, rinsed with 70% (v/v) ethanol, and dried.

## *In vitro* tRNA cleavage assay

The standard tRNA cleavage activity assay was conducted at 37°C, in a reaction mixture containing 20 mM Tris–Cl, pH 7.4 150 mM NaCl,1 mM $MgCl_2$, 1 μM tRNA, 0.1 μM CysK and 0.1 μM CdiA-$CT^{EC536}$. The specific conditions for each assay of tRNA cleavage by CdiA-$CT^{EC536}$ are clearly described in either the text or figure legends. Reactions were quenched by the addition of an equal volume of formamide gel-loading buffer, containing 95% (v/v) formamide, 0.02% (w/v) SDS, 0.02% (w/v) bromophenol blue and 0.01% (w/v) xylene cyanol, and the tRNAs were separated by 10% (w/v) polyacrylamide gel electrophoresis (PAGE) under denaturing conditions. The gels were stained with ethidium bromide, and tRNA band intensities were quantified by the Image Lab software (Bio-Rad, version 3.0).

## Mapping of tRNA cleavage site

The 5′-phosphate of *E. coli* $tRNA^{Ile}GAU$, purified as described above, was dephosphorylated by alkaline phosphatase from *E. coli* C75 (TAKARA, Japan), and then extracted with phenol-chloroform-isoamyl alcohol (25:24:1) (Nippongene, Japan). The tRNA was ethanol-precipitated, rinsed with 70% (v/v) ethanol, and dried. Subsequently, the 5′-end of $tRNA^{Ile}GAU$ was $^{32}P$-labeled by T4 polynucleotide kinase (TAKARA, Japan) using γ-$^{32}P$-ATP (3000 Ci/mmol, PerkinElmer, Japan), phenol-chloroform-isoamyl alcohol extracted, ethanol-precipitated, rinsed with 70% ethanol, and dried. $^{32}P$-labeled $tRNA^{Ile}GAU$ was separated by PAGE under denaturing conditions. The band containing $^{32}P$-labeled $tRNA^{Ile}GAU$ was excised, and the tRNA was eluted from the gel, ethanol-precipitated, rinsed with 70% (v/v) ethanol and dried. The $^{32}P$-$tRNA^{Ile}GAU$ (5 000 cpm) was cleaved in a reaction mixture, containing 20 mM Tris-Cl, pH 7.4, 150 mM NaCl, 1 mM $MgCl_2$, 1 μM unlabeled $tRNA^{Ile}GAU$, 0.1 μM CysK and 0.1 μM CdiA-$CT^{EC536}$, at 37°C for 5 min. The RNase T1 (Invitrogen, Japan) cleavage and alkaline hydrolysis cleavage sequence ladders of $^{32}P$-labeled $tRNA^{Ile}GAU$ were used as references to determine the site cleaved by CdiA-$CT^{EC536}$. The gel was exposed to an imaging plate and analyzed using a BAS-2000 imager (FujiFilm, Japan).

## *In vivo* toxicity assay

The *E. coli* MG1655 strain was transformed with pBAD_CdiA-$CT^{EC536}$_ΔI227 or its variants, inoculated in LB containing 50 μg/mL chloramphenicol and 1% (w/v) glucose, and cultured overnight at 37°C. The overnight culture was diluted serially, and aliquots (3 μl) were spotted onto LB plates containing 50 μg/mL chloramphenicol and 0.2% (w/v) arabinose or 1% (w/v) glucose, and the plates were incubated overnight at 37°C. Since the pBAD33 vector encoding wild-type CdiA-$CT^{EC536}$ was not obtained due to the wild-type CdiA-$CT^{EC536}$ toxicity, CdiA-$CT^{EC536}$ with the C-terminal I227 deletion was used as the 'wild-type', and each mutant is derived from wild (Δ_I227) in Figures 3 and 5.

## Northern blotting

*E. coli* strain MG1655 was transformed by pBAD33_CdiA-$CT^{EC536}$ or its variants, inoculated in LB containing 30 μg/ml chloramphenicol and 1% (w/v) glucose, and cultured at 37°C overnight. The overnight cultures were diluted into fresh liquid LB (4 ml) containing 30 μg/ml chloramphenicol to an $OD_{660}$ of 0.02 and incubated at 37°C until the $OD_{660}$ reached ∼0.2. Then, 0.2% (w/v) arabinose was added and after the culture was continued for 1 h at 37°C, the cells were harvested. Total RNAs were prepared using ISOGEN II (Nippongene, Japan), and the RNAs were separated by 10% (w/v) PAGE under denaturing conditions. RNAs were transferred to a Hybond-N + membrane (GE Healthcare, Japan). Hybridization was performed overnight at 60°C in PerfectHyb Hybridization Solution (Toyobo, Japan), using 5′-$^{32}P$-labeled oligonucleotide probes specific to each tRNA (20). After hybridization, the membrane was washed with buffer containing 2 × saline sodium citrate (SSC) and 0.1% (w/v) SDS for 5 min (three times), and then washed with buffer containing 0.1× SSC and 0.1% (w/v) SDS for 10 min at 60°C (twice). The membranes were exposed to the imaging plate and analyzed using a BAS-2000 imager (FujiFilm, Japan). The oligonucleotide sequences used as specific probes for tRNAs are listed in Supplementary Table 2, and the nucleotide sequences of tRNAs are listed in Supplementary Table 3.

## Pull-down assay

*E. coli* strain BL21(DE3) was transformed by pETDuet-CysK-CdiA-$CT^{EC536}$_H178A or its variants with C-terminal amino acid deletions, and cultured until the $OD_{660}$ reached ∼0.8. Protein expression was induced by adding 0.1 mM IPTG, and the culture was continued for 4 h at 37°C. The harvested cells were sonicated in buffer A supplemented with 0.1 mM PMSF and 50 μg/ml lysozyme, and the lysates were centrifuged. The supernatants were loaded onto a Ni-NTA agarose column, which was washed with buffer A, and the proteins were eluted from the column with buffer B. The eluted proteins were separated on a 12.5% SuperSep gel (Wako, Japan) and stained with Coomassie Brilliant Blue (CBB).

### Grid preparation.

The CysK:CdiA-CT$^{EC536}$_H178A complex (6 μM), purified as described above, was mixed with *E. coli* tRNA$^{Ile}$ GAU (6.6 μM) in buffer containing 25 mM Tris-HCl, pH 7.0, 50 mM NaCl, 2 mM $MgCl_2$ and 10 mM β-mercaptoethanol. The mixture was incubated at 37°C for 20 min and then placed on ice for 10 min prior to grid preparation. A Quantifoil Cu R1.2/1.3 200 mesh grid (Quantifoil) was glow-discharged at 8 mA for 30 s, using a PIB-10 Plasma Ion Bombarder (Vacuum Device). The sample (0.4 mg/ml) was applied onto the grid at 100% humidity at 4°C with a blot force of 10 for 4 s, and then the grid was plunge frozen in liquid ethane using a Mark IV Vitrobot (ThermoFisher Scientific). Cryo-EM movies were collected on a Thermo Scientific™ Titan Krios G3i transmission electron microscope equipped with a K3 direct electron detector (Gatan, Inc.) operated at 300 kV. In total, 7044 micrographs were collected with a pixel size of 0.83 Å and a total dose of 50 electrons/Å$^2$.

### Cryo-EM image processing

Cryo-EM workflows are shown in Supplementary Figures 1 and 2. Cryo-EM image processing was performed in CryoSPARC (ver. 4.3.1) (27). Movie stacks were motion corrected (28) and contrast-transfer functions (CTFs) were estimated. Particles were blob-based autopicked. Several rounds of reference-free two-dimensional (2D) classification were performed and particles were manually separated into two classes: with and without nucleic acid-like features. Clean particle stacks were 3D reconstructed using non-uniform refinement (29) and polished by local contrast transfer function (CTF) refinement (30) to a resolution of 2.83 Å. Two conformations were identified by 3D classification (complex-A and -B). The final reconstructions for the two conformations were performed by non-uniform refinement. The generated maps were polished by DeepEMhancer (ver. 0.14) (31) and the final resolutions for complex-A and -B were 2.99 and 3.04 Å, respectively (Table 1, Supplementary Table 4).

### Model building and refinements

The starting model was assembled from the CysK:CdiA-CT$^{EC536}$ structure (PDB ID: 5J43)(13) and *E. coli* tRNA $^{Ile}$ GAU (PDB ID: 1QU2). These models were body fitted into each cryo-EM density map using ChimeraX (ver. 1.6.1) (32) and the structure was refined using phenix.real_space_refine (33,34), and then manually corrected with Coot (ver. 0.9) (35).

**Table 1.** Cryo-EM data collection, refinement and validation statistics

| | #1 CysK:CdiA-CT$^{EC536}$:tRNA complex-A (EMDB-60561) (PDB 8ZYC) |
|---|---|
| **Data collection and processing** | |
| Magnification | 105 000 |
| Voltage (kV) | 300 |
| Electron exposure (e$^-$/Å$^2$) | 50 |
| Defocus range (μm) | −0.8 to −1.8 |
| Pixel size (Å) | 0.83 |
| Symmetry imposed | C1 |
| Initial particle images (no.) | 4 707 496 |
| Final particle images (no.) | 115 994 |
| Map resolution (Å) | 2.99 |
| FSC threshold | 0.143 |
| **Refinement** | |
| Initial model used (PDB code) | 5J43 |
| Model resolution (Å) | 3.1 |
| FSC threshold | 0.5 |
| Map sharpening *B* factor (Å$^2$) | −89 |
| Model composition | |
| Non-hydrogen atoms | 7058 |
| Protein residues | 728 |
| RNA residues | 72 |
| Magnesium ion | 2 |
| *B* factors (Å$^2$) | |
| Protein | 51.25 |
| RNA | 116.57 |
| Magnesium ion | 72.80 |
| R.m.s. deviations | |
| Bond lengths (Å) | 0.008 |
| Bond angles (°) | 0.835 |
| Validation | |
| MolProbity score | 1.44 |
| Clashscore | 4.45 |
| Poor rotamers (%) | 0.35 |
| Ramachandran plot | |
| Favored (%) | 96.65 |
| Allowed (%) | 3.35 |
| Disallowed (%) | 0.00 |

## Results

### CdiA-CT$^{EC536}$ cleaves tRNA between nucleotides 32 and 33

Wild-type CdiA-CT$^{EC536}$ was co-expressed with the CdiI$^{EC536}$ immunity protein and the CdiA-CT$^{EC536}$:CdiI $^{EC536}$ complex was first purified, since the expression of wild-type CdiA-CT$^{EC536}$ alone is toxic to *E. coli*. After denaturing the CdiA-CT$^{EC536}$:CdiI $^{EC536}$ complex and separating CdiA-CT$^{EC536}$ from CdiI $^{EC536}$, CdiA-CT$^{EC536}$ was refolded and further purified as described in the Methods.

While tRNA (tRNA$^{Ile}$GAU purified from *E. coli*) is not cleaved in the presence of CdiA-CT$^{EC536}$ alone, it is cleaved in the presence of both CdiA-CT$^{EC536}$ and CysK (Figure 1A). tRNA cleavage in the presence of CysK and CdiA-CT$^{EC536}$ was blocked by the addition of CdiI $^{EC536}$ to the reaction (Figure 1B). Thus, tRNA cleavage is caused by CdiA-CT$^{EC536}$ and activated by CysK, in agreement with the previous report (13,15).

To clarify the site in tRNA$^{Ile}$GAU that is cleaved by CdiA-CT$^{EC536}$ in the presence of CysK, 5′-$^{32}$P-labeled tRNA$^{Ile}$GAU was cleaved by CdiA-CT$^{EC536}$ in the presence of CysK, and the cleavage site was mapped by referring to the limited alkaline ladder and RNase T1 digests of 5′-$^{32}$P-labeled tRNA$^{Ile}$GAU separated by PAGE (Figure 1C). The result showed that tRNA$^{Ile}$GAU was cleaved between the nucleotides at positions 32 (C32) and 33 (U33) (Figure 1C). The 5′ terminus of the 3′-half of tRNA$^{Ile}$GAU was 5′-$^{32}$P-labeled by T4 polynucleotide kinase without prior dephosphorylation by alkaline phosphatase (Figure 1D). Thus, the 5′-terminus of the 3′-half is a hydroxyl group. The 3′ terminus of the 5′-half of tRNA$^{Ile}$GAU would be a 2′,3′-cyclic phosphate. CdiA-CT$^{EC536}$ is thus a typical ribonuclease generating a 2′,3′-cyclic phosphate and a 5′-hydroxyl group at the 3′-end of the 5′-half and the 5′-end of the 3′-half, respectively.

### Structural analysis of the CysK:CdiA-CT$^{EC536}$:tRNA complex

To clarify the mechanism of tRNA recognition and cleavage by CdiA-CT$^{EC536}$ in the presence of CysK, the

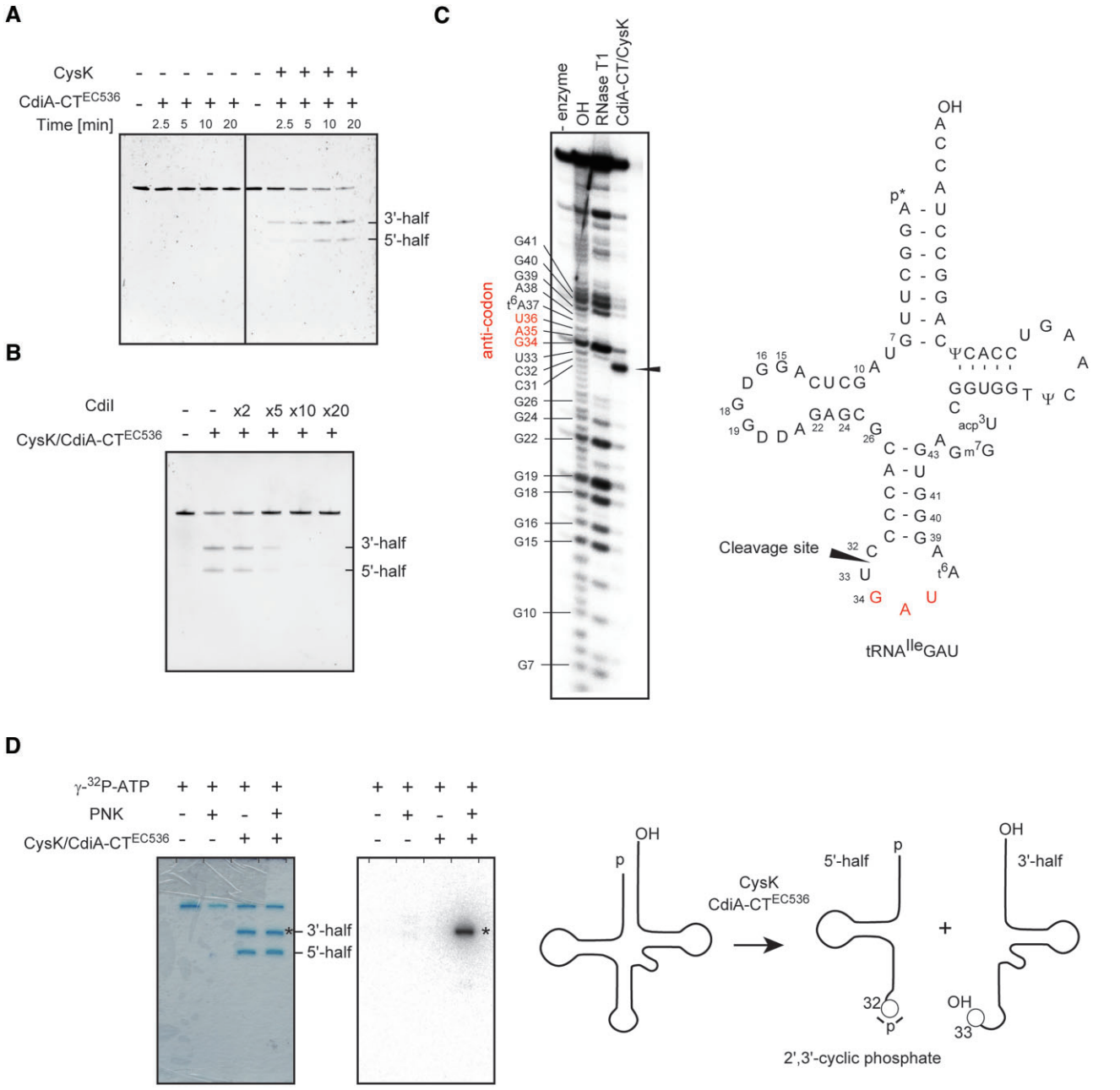


**Figure 1.** CdiA-CT$^{EC536}$ cleaves tRNA between nucleotides 32 and 33 in the presence of CysK. (**A**) tRNA cleavage by CdiA-CT$^{EC536}$ requires CysK. 1.0 μM tRNA$^{Ile}$GCU was incubated with 0.01 μM CdiA-CT$^{EC536}$ in either the absence or presence of 0.01 μM CysK at 37°C, in buffer containing 20 mM Tris–Cl, pH 7.4, 150 mM NaCl, 1 mM $MgCl_2$. (**B**) tRNA cleavage by CdiA-CT$^{EC536}$ in the presence of CysK was suppressed by adding CdiI immunity protein. 1.0 μM tRNA$^{Ile}$GCU was incubated with 0.1 μM CdiA-CT$^{EC536}$, 0.1 μM CysK and increasing amounts (0.2, 0.5, 1.0 and 2.0 μM) of CdiI at 37°C for 30 min in the same buffer as in (A). (**C**) CdiA-CT$^{EC536}$ cleaves tRNA$^{Ile}$GCU between the nucleotides at positions 32 and 33. 5′-$^{32}$P labeled tRNA$^{Ile}$GCU was cleaved by CdiA-CT$^{EC536}$:CysK. OH and RNaseT1 indicate samples digested with alkali and RNase T1, respectively. The arrow indicates the cleavage site in tRNA$^{Ile}$GCU and the numbering system of tRNA conforms to the proposal by Sprinzel *et al.* (55) (**D**) The 5′-end of the 3′-half fragment has a hydroxyl group. The 5′-end of the 3′-half of tRNA is phosphorylated by PNK without prior dephosphorylation by alkaline phosphatase. The 3′-end of the 5′-half would be a 2′,3′-cyclic phosphate.

catalytically inert H178A mutant CdiA-CT$^{EC536}$ (CdiA-CT$^{EC536}$_H178A) and CysK were co-expressed and the CysK:CdiA-CT$^{EC536}$_H178A (hereafter referred as CysK:CdiA-CT$^{EC536}$ for simplicity, unless otherwise stated) complex was purified. Our extensive crystallization trial of the CysK:CdiA-CT$^{EC536}$:tRNA ternary complex was not successful. A previous crystallographic analysis of the CysK:CdiA-CT$^{EC536}$ complex (PDB ID: 5J43) (13) showed that two CdiA-CT$^{EC536}$ molecules bind to a CysK dimer, forming a 2:2 CysK:CdiA-CT$^{EC536}$ complex. Thus, we expected that two tRNA molecules would bind to the 2:2 CysK:CdiA-CT$^{EC536}$ complex, forming the 2:2:2 CysK:CdiA-CT$^{EC536}$:tRNA ternary complex, and the size of the complex would be amenable for cryo-EM single particle analysis. Since a stable CysK:CdiA-CT$^{EC536}$:tRNA complex was not observed in the size-exclusion chromatography (SEC) anal-

ysis, the purified CysK:CdiA-CT$^{EC536}$ complex was mixed with tRNA (tRNA$^{Ile}$GAU isolated from *E. coli*) and the grid was prepared.

While the processing of cryo-EM micrographs and particle images showed one class exhibiting stoichiometries of a 2:1:1 CysK:CdiA-CT$^{EC536}$:tRNA ternary complex, the 2:2:2 CysK:CdiA-CT$^{EC536}$:tRNA complex was barely observed (Supplementary Figure 1). This could be due to the preparation of CysK:CdiA-CT$^{EC536}$ complexes, which might have included two classes, 2:2 and 2:1 CysK:CdiA-CT$^{EC536}$ complexes, and/or CdiA-CT$^{EC536}$ may have dissociated from the CysK dimer. As a result, the 2:1:1 CysK:CdiA-CT$^{EC536}$:tRNA complex was predominantly observed. 3D classification of the 2:1:1 CysK:CdiA-CT$^{EC536}$:tRNA complex resulted in two complexes (complexes A and B) (Supplementary Figure 1). The orientation of tRNA binding to CdiA-CT$^{EC536}$ differs between the two complexes, and in complex-A the anticodon region of tRNA is closer to the active site of CdiA-CT$^{EC536}$, as described below (Supplementary Figure 3). Therefore, to model the CysK:CdiA-CT$^{EC536}$:tRNA complex, we focused on the 2:1:1 CysK:CdiA-CT$^{EC536}$:tRNA complex-A (Figure 2A, Table 1). In addition to the 2:1:1 CysK:CdiA-CT$^{EC536}$:tRNA ternary complexes, processing of cryo-EM micrographs and particle images showed the 2:2 and 2:1 CysK:CdiA-CT$^{EC536}$ binary complexes as well (Supplementary Figure 2, Supplementary Table 4).

CdiA-CT$^{EC536}$ is composed of two domains. The N-terminal domain of CdiA-CT$^{EC536}$ reportedly controls the transport of the toxin into target bacteria, while the C-terminal domain is responsible for the toxicity and tRNase activity of CdiA-CT$^{EC536}$ (36). After CdiA-CT$^{EC536}$ is delivered into the periplasm, the N-terminal domain binds to specific inner membrane components for subsequent translocation into the cytoplasm.

In the 2:1:1 CysK:CdiA-CT$^{EC536}$:tRNA complexes and the 2:2 and 2:1 CysK:CdiA-CT$^{EC536}$ complexes, the maps corresponding to the N-terminal region (residues 1 – 126) of CdiA-CT$^{EC536}$ were not observed (Supplementary Figures 1 and 2), as in the crystallographic analysis of 2:2 CysK:CdiA-CT$^{EC536}$ complex (PDB ID 5J43) (13), suggesting the movement of the N-terminal region of CdiA-CT$^{EC536}$, even in the complex with tRNA.

## Overall structure of the CysK:CdiA-CT$^{EC536}$:tRNA ternary complex

In the 2:1:1 CysK:CdiA-CT$^{EC536}$:tRNA complex, CdiA-CT$^{EC536}$ interacts with one subunit of the CysK dimer (CysKa) and tRNA exclusively interacts with CdiA-CT$^{EC536}$, while there is no interaction between tRNA and CysK (Figure 2A, Supplementary Figure 4A).

The tRNA binding area on CdiA-CT$^{EC536}$ overlaps with the CdiI $^{EC536}$ binding area on CdiA-CT$^{EC536}$ (PDB ID 5J5V) (13) (Figure 2B). Thus, the immunity protein CdiI $^{EC536}$ functions to block tRNA binding to CdiA-CT$^{EC536}$, thereby inhibiting tRNA cleavage by CdiA-CT$^{EC536}$. A comparison of the structures of CdiA-CT$^{EC536}$ in the CysK:CdiA-CT$^{EC536}$:tRNA ternary complex and CysK:CdiA-CT$^{EC536}$ binary complex (PDB ID 5J43) (13) showed that the loop between α2 and α3 of CdiA-CT$^{EC536}$ is pushed toward CysK upon tRNA binding to CdiA-CT$^{EC536}$ (Figure 2C). The similar loop movement was also observed in the CysK:CdiA-CT$^{EC536}$:CdiI ternary complex (13). Thus, the movement of the loop upon tRNA binding to CdiA-CT$^{EC536}$ is facilitated by the tight interaction between CdiA-CT$^{EC536}$ and CysK, as described below.

The C-terminal region, including the C-tail (residues 224–227) followed by α4 of CdiA-CT$^{EC536}$, interacts with CysK via hydrophobic interactions (Figure 3A), as observed in the crystal structure of the CysK:CdiA-CT$^{EC536}$ complex (13). The C-terminal I227 residue stacks with the PLP (*N*′-pyridoxyl-lysine-5′-monophosphate) and is surrounded by hydrophobic residues, F144 and F234, and the main chain of the C-tail interacts with M120 through hydrophobic interactions (Figure 3A). The I157 in α2 of CdiA-CT$^{EC536}$ interacts with T95 in CysK through hydrophobic interaction. The Y225 residue is stacked with L160 in α2 of CdiA-CT$^{EC536}$ and the OH group of Y225 hydrogen-bonds with D164, located at the C-end of α2 in CdiA-CT$^{EC536}$, bridging the α2 and α4 helices. Y225 also hydrogen-bonds with T95 in CysK. K166, in the loop between α2 and α3 of CdiA-CT$^{EC536}$, hydrogen-bonds with S97 and S308 in CysK, and Q183 in α3 of CdiA-CT$^{EC536}$ hydrogen-bonds with D207 in CysK (Figure 3B).

The interaction between CdiA-CT$^{EC536}$ and CysK would assist in bundling the α-helices of the C-terminal domain (α2, α3 and α4) of CdiA-CT$^{EC536}$, thus stabilizing its structure. A previous study analyzed the thermal stability of CdiA-CT$^{EC536}$ in the presence and absence of CysK using circular dichroism (CD) spectroscopy and differential scanning fluorimetry (DSF). The results showed that the CysK:CdiA-CT$^{EC536}$ complex is more stable than the individual components, suggesting that CdiA-CT$^{EC536}$ is intrinsically less stable and gains thermostability when bound to CysK. The interactions between CdiA-CT$^{EC536}$ and CysK also provide a stable foundation for the formation of catalytic sites in CdiA-CT$^{EC536}$ (Figures 2C and 3A, B).

Since the structure of *apo* CdiA-CT$^{EC536}$ is not available, the *apo* CdiA-CT$^{EC536}$ (amino acid residues 127–227) was modeled using AlphaFold2 (37). AlphaFold predicted possible alternative structures of *apo* CdiA-CT$^{EC536}$ (Supplementary Figure 5). Comparison of the AlphaFold-models of *apo* CdiA-CT $^{EC536}$ suggests that the N-terminal alpha helical region (amino acids 134 – 163) could adopt the alternative conformations. One has an extended long helix (A1), and the others have a bent conformation with two helices (α1 and α2). The N-terminal region of CdiA-CT$^{EC536}$ structure in the CysK:CdiA-CT$^{EC536}$:tRNA ternary complex adopts the bent conformation with the two helices. Thus, CdiA-CT$^{EC536}$ binding to CysK would transit and fix the N-terminal region of CdiA-CT$^{EC536}$conformation to the bent conformation (Figure 3C) and the interactions between α2, α3 and α4 are strengthened, stabilizing the CdiA-CT$^{EC536}$ structure (Figure 3A,B). The $Mg^{2+}$-coordinating D155, which is required for activity as described below, is located between α1 and α2. Thus, the binding of CdiA-CT$^{EC536}$ to CysK facilitates the formation of the catalytic active site, consisting of α2 and the loop between α2 and α3, in CdiA-CT$^{EC536}$, thereby promotes the catalysis upon tRNA binding to CdiA-CT$^{EC536}$ for tRNA cleavage (Figures 2C and 3D). Altogether, CysK provides the platform for CdiA-CT$^{EC536}$ to cleave substrate tRNAs.

## CysK:CdiA-CT$^{EC536}$ interaction and CdiA-CT$^{EC536}$ activity

To assess the involvement of the C-terminal tail of CdiA-CT$^{EC536}$ (Figure 3A) in its activity and toxicity, CdiA-CT$^{EC536}$

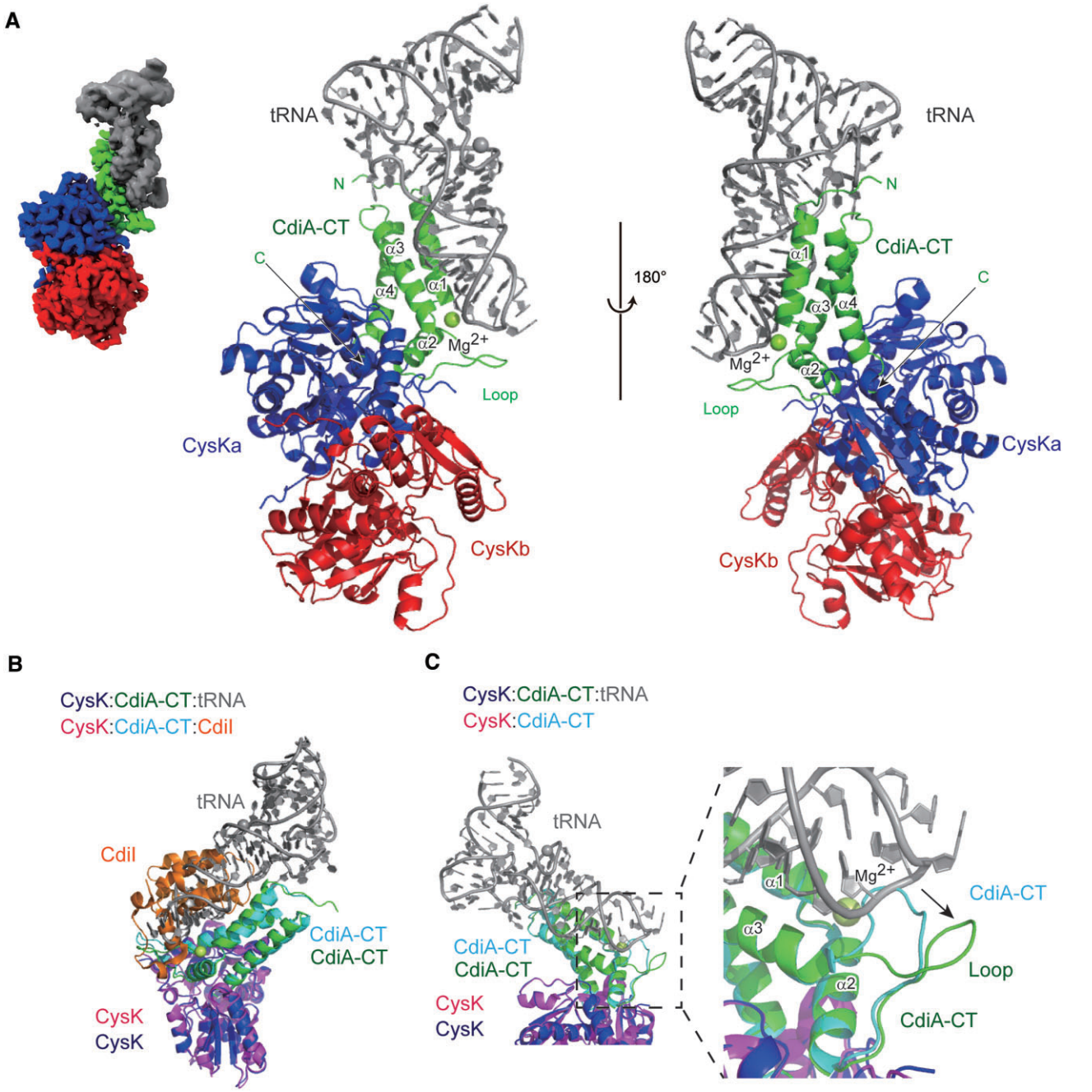


**Figure 2.** Overall structure of CysK:CdiA-CT$^{EC536}$:tRNA complex. (**A**) Overall structure of the 2:1:1 CysK:CdiA-CT$^{EC536}$:tRNA complex-A. CdiA-CT$^{EC536}$ (green), CysK (blue and red) and tRNA (gray) are shown. (**B**) The CdiI$^{EC536}$ immunity protein binding site on CdiA-CT$^{EC536}$ overlaps with the tRNA anticodon stem-loop binding site on CdiA-CT$^{EC536}$. The subunits of CysK:CdiA-CT$^{EC536}$:tRNA are colored as in (A). The subunits of CysK:CdiA-CT$^{EC536}$:CdiI (PDB ID 5J5V) (13) are colored magenta, cyan, and orange, respectively. (**C**) Conformational change of the loop between α2 and α3 upon tRNA binding to CdiA-CT$^{EC536}$. CdiA-CT$^{EC536}$ in CysK:CdiA-CT$^{EC536}$ (PDB ID 5J43) and CysK:CdiA-CT$^{EC536}$:tRNA are colored cyan and green, respectively.

mutants were expressed in *E. coli* and their toxicity was evaluated. While the mutant CdiA-CT$^{EC536}$_GYG- (Δ1), with the C-terminal I227 deletion, is toxic in *E. coli*, the other C-terminal tail deletion mutants, CdiA-CT$^{EC536}$_GY– (Δ2), CdiA-CT$^{EC536}$_G– (Δ3) and CdiA-CT$^{EC536}$– (Δ4), showed attenuated toxicity as compared with CdiA-CT$^{EC536}$_GYG- (Δ1) (Figure 4A). Consistent with the lower toxicity of CdiA-CT$^{EC536}$ mutants with serial deletions of the C-terminal residues, tRNA fragmentation in *E. coli* upon expression of these mutants decreased (Figure 4B), and tRNA cleavage was not observed when CdiA-CT$^{EC536}$—- (Δ4) was expressed. Thus, the toxicity of CdiA-CT$^{EC536}$ and the tRNA cleavage in *E. coli* are correlated *in vivo*. To assess the involvement of the C-tail of CdiA-CT$^{EC536}$ for complex formation with CysK *in vivo*, the interactions between CysK and the CdiA-CT$^{EC536}$ mutants with C-terminal tail deletions were evaluated by pull-down assays, using cell extracts from *E. coli* expressing both CysK and N-terminal histidine-tagged CdiA-CT$^{EC536}$_H178A variants (Figure 4C). While CdiA-CT$^{EC536}$_H178A with the GYGI tail was co-purified with CysK even under stringent conditions (high salt buffer containing 500 mM NaCl), CdiA-CT$^{EC356}$_H178A with deletions of C-terminal tail residues,

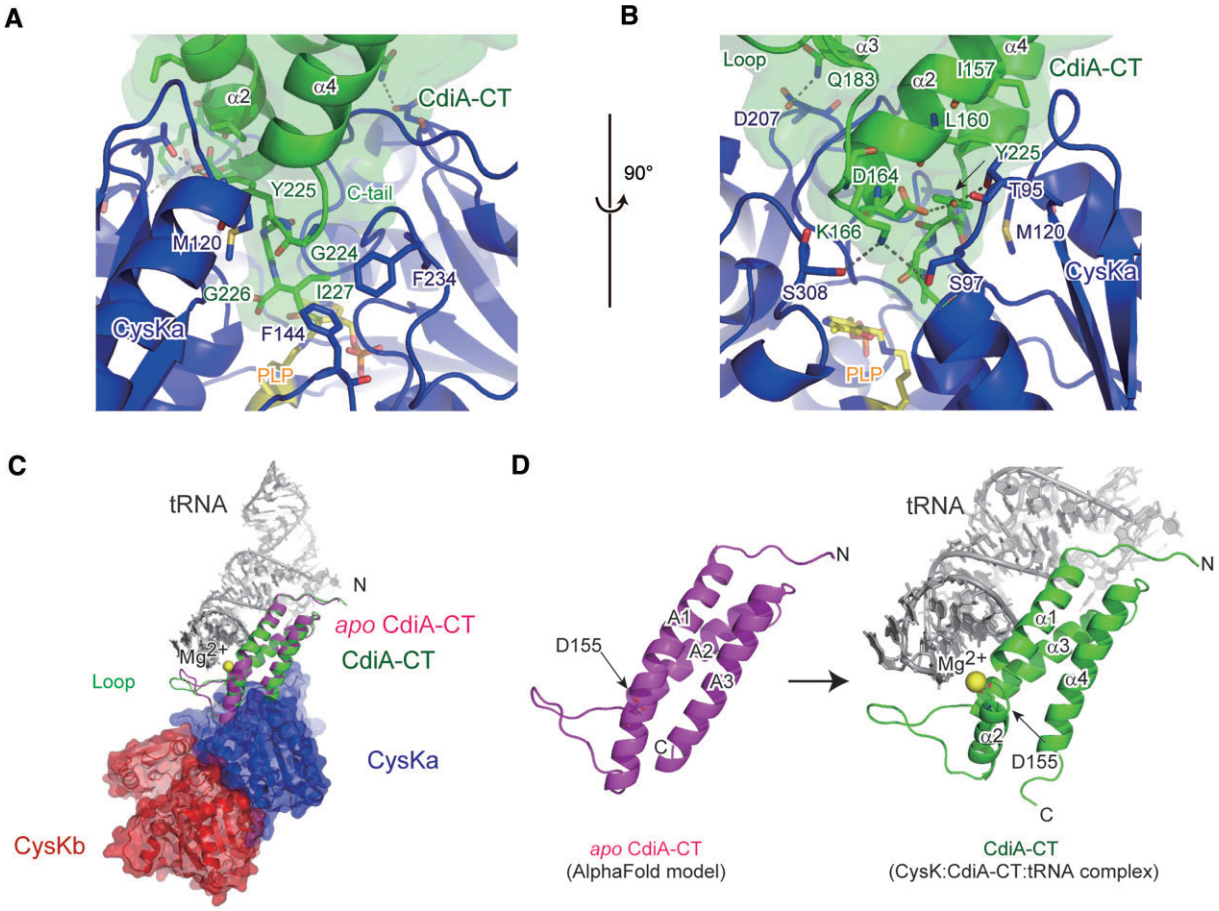


**Figure 3.** Interaction between CysK and CdiA-CT$^{EC536}$. (**A, B**) Interactions between CdiA-CT$^{EC536}$ (green) and CysK (blue). PLP (N′-pyridoxyl-lysine-5′-monophosphate) is shown as a yellow stick model. (**C**) An AlphaFold model of *apo* CdiA-CT$^{EC536}$ (amino acid residues 127–227; magenta) with a bent conformation was superimposed onto the CdiA-CT$^{EC536}$ (green) in the CysK:CdiA-CT$^{EC536}$ ternary complex. CysKs are colored red and blue, and tRNA is colored gray. (**D**) Comparison of *apo* CdiA-CT$^{EC536}$ (left, magenta) and its complex (right, green) with CysK. $Mg^{2+}$ ion (colored yellow) is coordinated to D155 in CdiA-CT$^{EC536}$ in complex with CysK.

the CdiA-CT$^{EC536}$ variants (Δ1−Δ4), did not co-purify with CysK (Figure 4C). In addition to the interactions between CysK and the C-tail of CdiA-CT$^{EC536}$ (Figure 3A), others between CdiA-CT$^{EC536}$ and CysK (Figure 3B) contribute to the toxicity and tRNA cleavage activity of CdiA-CT$^{EC536}$ *in vivo*. Mutations of the residues that interact with CysK and bridge the α-helices of CdiA-CT$^{EC536}$, I157A, L160A, K161A, D164A, K166A, Q183A and Y225A, attenuated the toxicity *in vivo* (Figure 4D). The I157A, L160A, K161A, D164A and Y225A mutations reduced the tRNA fragmentation significantly, while K166A and Q183A reduced it to a lesser extent when the mutants were expressed in *E. coli* (Figure 4E). Altogether, CysK:CdiA-CT$^{EC536}$ complex formation is required for the tRNA cleavage and toxicity of CdiA-CT$^{EC536}$.

## tRNA recognition by CdiA-CT$^{EC536}$

As described above, in the CysK:CdiA-CT$^{EC536}$:tRNA complex, the tRNA exclusively interacts with CdiA-CT$^{EC536}$ and does not interact with CysK (Figures 2A and 5A).

The bottom half of the tRNA – D-stem-loop and anticodon stem-loop interact with CdiA-CT$^{EC536}$ (Figure 5A–C), while the top half of the tRNA (acceptor and TΨC stem-loop) does not. The α1 helix of CdiA-CT$^{EC536}$ interacts with the helical structure of the bottom half of the tRNA (Figure 5A, B, Supplementary Figure 4B, C), engaging with the minor and major grooves. Thus, CdiA-CT$^{EC536}$ recognizes the structures of the D stem-loop and anticodon stem-loop of tRNA. As a result, the anticodon loop of tRNA is placed in the active pocket of CdiA-CT$^{EC536}$, which is formed by α2 and the loop between α2 and α3 of CdiA-CT$^{EC536}$ (Figures 2C and 3D).

The side chain of Q134 protrudes into the minor groove of the D-stem and hydrogen-bonds with the 2-$NH_2$ group of G22 of tRNA (Figure 5A–C). The N133 residue hydrogen-bonds with the 6-O atom of G16, and K135 interacts with the phosphate of G22. The side chain of K142 protrudes toward the major groove between the D-stem and anticodon stem and interacts with the phosphate backbones of G24 and G41 (Figure 5A, C), while S138 also hydrogen-bonds with the phosphate of G24. The C-terminal half of α1 and α3 interact with the minor groove of the anticodon stem region of tRNA. N145 on α1 interacts with the phosphate backbone of G40, and N149 hydrogen-bonds with the ribose 4 atom of G39 (Figure 5D). Q180 and R187 on α3 form hydrogen bonds with the 2′-OH groups of the C30 ribose and G41 ribose, respectively, and N191 hydrogen-bonds with the phosphate of U42 (Figure 5D). The nucleotides around the tRNA cleavage site are proximal to the loop between α2 and α3 of CdiA-CT$^{EC536}$. One $Mg^{2+}$ ion is coordinated by D155 and is close to

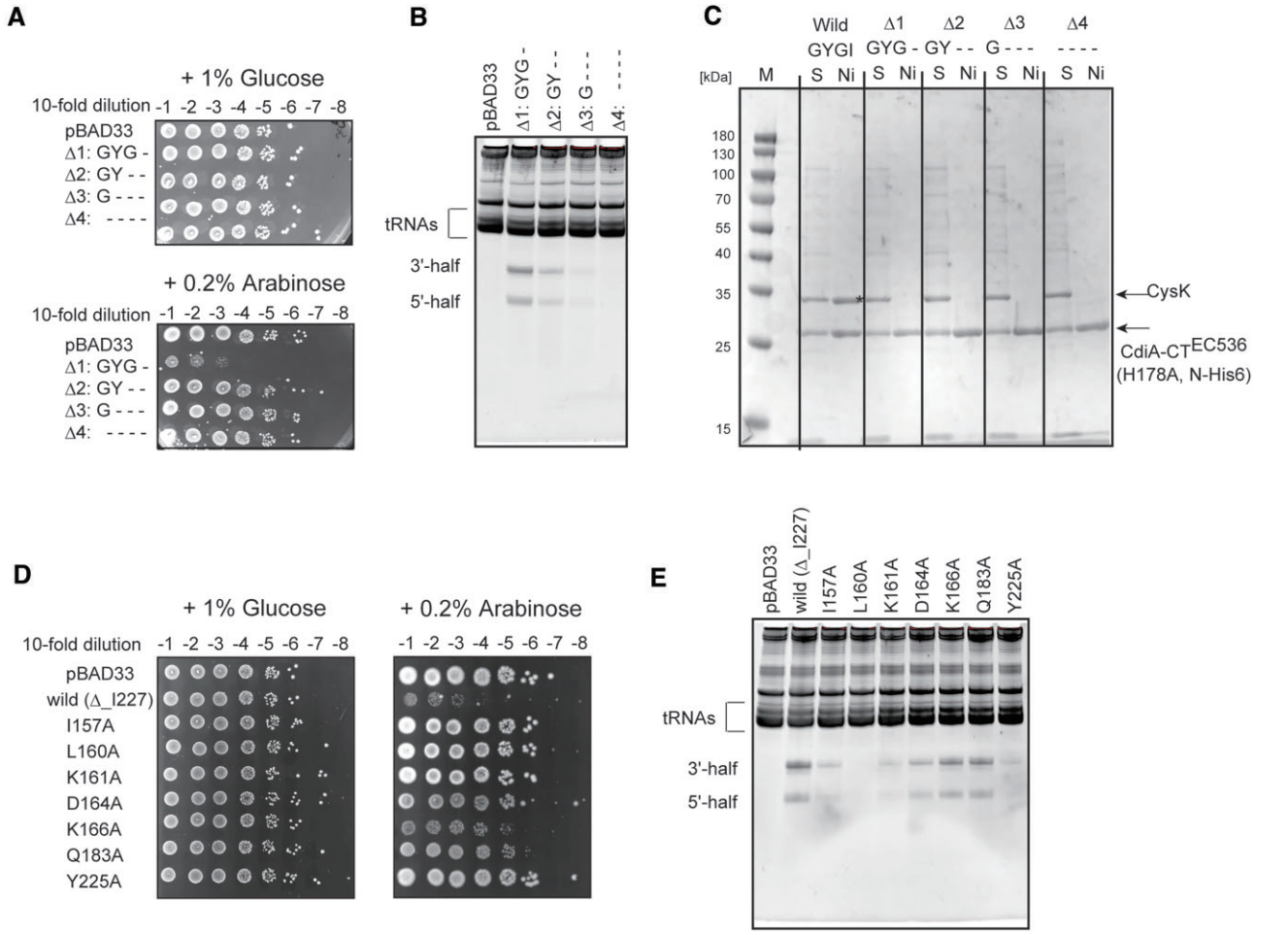


**Figure 4.** CysK:CdiA-CT$^{EC536}$ interaction facilitates tRNA cleavage and toxicity *in vivo*. (**A**) The deletion of the C-terminal tail attenuated the toxicity of CdiA-CT$^{EC536}$ *in vivo*. Overnight cultures of *E. coli* MG1655 transformed with pBAD33, pBAD_CdiA-CT$^{EC536}$_GYG- (Δ1), pBAD_CdiA-CT$^{EC536}$_GY– (Δ2), pBAD_CdiA-CT$^{EC536}$_G— (Δ3) and pBAD_CdiA-CT$^{EC536}$_—— (Δ4) were serially diluted, and aliquots were spotted on LB plates containing 50 μg/mL chloramphenicol supplemented with either 1% (w/v) glucose (upper panel) or 0.2% (w/v) arabinose (lower panel). The plates were incubated at 37°C overnight. (**B**) tRNA cleavage is attenuated as the C-terminal tail is deleted *in vivo*. The expression of the C-terminal deletion mutants of CdiA-CT$^{EC536}$ in (A) was induced in MG1655 by adding 0.2% (w/v) arabinose for 1 h at 37°C. RNAs were prepared and separated by 10% (w/v) PAGE under denaturing conditions, and the gel was stained with ethidium bromide. (**C**) Pull-down of CysK and CdiA-CT$^{EC536}$_H178A and its variants (Δ1–Δ4). CysK and N-terminally histidine-tagged CdiA-CT$^{EC536}$_H178A or its variants were co-expressed in *E. coli* BE21(DE3) and the lysates were applied to a Ni-NTA column. The column was washed, and the histidine tagged CdiA-CT$^{EC536}$_H178A or its variants was eluted from the column. 'S' and 'Ni' represent the supernatant of the cell lysates and the eluted proteins from the Ni-NTA column, respectively. (**D**) Mutations of the CysK interacting residues in CdiA-CT$^{EC536}$ attenuated the toxicity of CdiA-CT$^{EC536}$ *in vivo*. (**E**) tRNA cleavage is attenuated by the presence of mutant of CdiA-CT$^{EC536}$ in (D) *in vivo*.

the 2′-OH of the C32 ribose (Supplementary Figure 4C), and W176 in the loop interacts with the phosphate of C32 (Figure 5D). E181 hydrogen-bonds with the 2′-OH of the C31 ribose. The $Mg^{2+}$ ion coordinated to D155, and the loop between α2 and α3 participate in the tRNA cleavage reaction, as described below.

To assess the involvement of the tRNA interacting amino acid residues in CdiA-CT$^{EC536}$ in its toxicity, CdiA-CT$^{EC536}$ mutants were expressed in *E. coli* and their toxicities were evaluated (Figure 6A). Mutations of the residues that interact with the D stem-loop and anticodon stem of tRNA, N133A, Q134A, S138A, K142A, N145A, N149A, Q180A and R187A, attenuated the toxicity *in vivo*. Furthermore, mutations of the residues in the loop between α2 and α3, K170A, W176A, H178A, D155A and E181, also reduced the toxicity *in vivo* (Figure 6A). Consistent with the weaker toxicities of the CdiA-CT$^{EC536}$ mutants when expressed in *E. coli*, tRNA fragmentation was decreased or abolished (Figure 6B).

## Catalytic mechanism of tRNA cleavage

CdiA-CT$^{EC536}$ reportedly required metal ions for its activity (13) (Figure 7A). Thus, it is likely that the $Mg^{2+}$ ion coordinated by D155 is involved in the catalysis. As described above, the D155A mutation of CdiA-CT$^{EC536}$ attenuated its tRNA cleavage activity and toxicity *in vivo* (Figure 6A, B). Furthermore, the loop mutations, W176A, H178A and K170A, also decreased the tRNA cleavage activity and toxicity *in vivo* (Figure 6A, B). The structure we determined is that of the catalytically inactive H178A mutant, CdiA-CT$^{EC536}$_H178A, in complex with CysK and tRNA. We modeled the H178 residue in the present structure of CysK:CdiA-CT$^{EC536}$:tRNA (Figure 7B). In the model, H178 is adjacent to the C32 ribose, while in the structure, $Mg^{2+}$, coordinated by D155 (Supplementary Figure 4C), is proximal to the 2′-OH group of the C32 ribose. This proximity suggests that $Mg^{2+}$ would facilitate the abstraction of a proton from the 2′-OH group of the C32 ribose, enabling the 2′-oxygen of the 2′-OH to

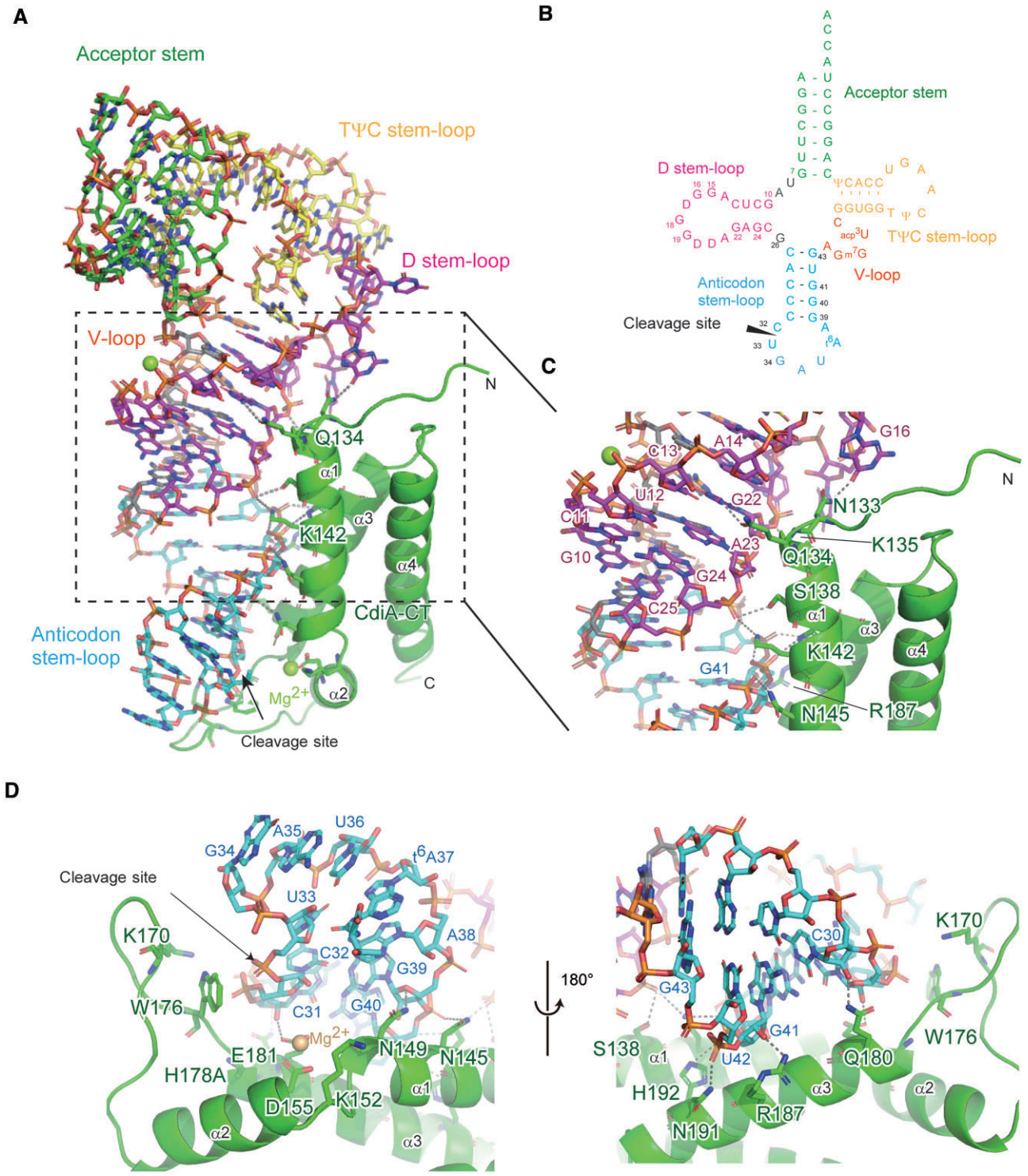


**Figure 5.** tRNA recognition by CdiA-CT$^{EC536}$. (**A**) CdiA-CT$^{EC536}$ interacts with only the bottom half of tRNA. For simplicity, only the tRNA (stick model) and CdiA-CT$^{EC536}$ (green) in the CysK:CdiA-CT$^{EC536}$:tRNA complex are shown. Acceptor-stem, D stem-loop, anticodon stem-loop, variable loop and TΨC stem-loop of tRNA are colored green, magenta, cyan, orange, and yellow, respectively. (**B**) *E. coli* tRNA$^{Ile}$GCU nucleotide sequence in a clover-form structure, with the Acceptor-stem, D stem-loop, anticodon stem-loop, variable loop and TΨC stem-loop colored as in (A). The site in tRNA cleaved by CdiA-CT$^{EC536}$ is depicted by a black arrow. (**C**) Close-up view of the interactions between CdiA-CT$^{EC536}$ (green) and the D stem-loop (magenta sticks) of tRNA. (**D**) Close-up view of the interactions between CdiA-CT$^{EC536}$ and the anticodon stem-loop (cyan sticks) of tRNA.

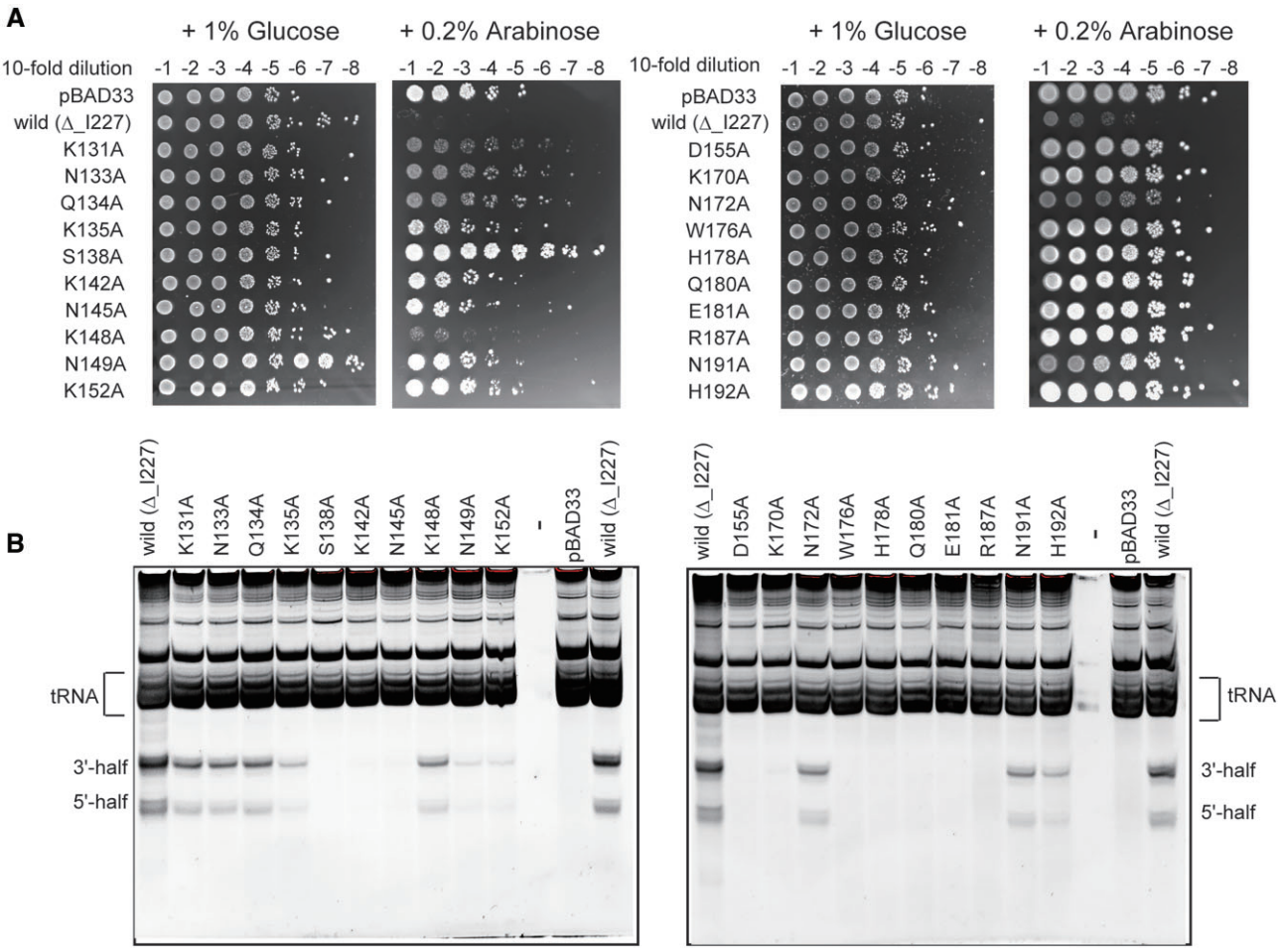


**Figure 6.** Correlation between CdiA-CT$^{EC536}$ toxicity and tRNA cleavage *in vivo*. (**A**) Mutations of the residues involved in the interaction with tRNA or catalysis attenuated the toxicity of CdiA-CT$^{EC536}$ when expressed in *E. coli*. The experimental procedures are the same as described in Figure 4A. (**B**) tRNA cleavage by CdiA-CT$^{EC536}$ and its variants in (A) expressed in *E. coli*. The experimental procedures are the same as described in Figure 4B.

nucleophilically attack the phosphorus atom between C32 and U33 (Figure 7C). The transition state, featuring a pentavalent phosphate, is stabilized by the interaction with the Nε atom of W176. Following this transition state, H178 would protonate the 5′-oxygen of the U33 ribose, leading to the formation of the 2′,3′-cyclic phosphate at the C32 ribose and the 5′-hydroxyl group at the 5′-terminus of C33.

## Discussion

Previous reports showed that CdiA-CT$^{EC536}$ binding to CysK stabilizes the CdiA-CT$^{EC536}$:CdiI complex (14), and that CdiA-CT $^{EC536}$ binding to CysK stabilizes the CdiA-CT$^{EC536}$ structure and enhances tRNA binding to CysK:CdiA-CT$^{EC536}$ (13). However, the mechanism of tRNA recognition and cleavage by the CysK:CdiA-CT$^{EC536}$ complex has remained elusive. In this study, we present the cryo-EM structure of the CysK:CdiA-CT$^{EC536}$:tRNA ternary complex (Figure 2, Supplementary Figure 4). The tRNA does not contact CysK, and the bottom-half of the tRNA is recognized by and interacts with only CdiA-CT$^{EC536}$ in the CysK:CdiA-CT$^{EC536}$ complex (Figures 2 and 5). The α-helices of CdiA-CT$^{EC536}$ clamp the minor and major grooves of the D-stem and anticodon stem of tRNA (Figure 5A), positioning the anticodon loop in the active site of CdiA-CT$^{EC536}$ for tRNA cleavage. The interaction between CysK and CdiA-CT$^{EC536}$ facilitates the stabilization of CdiA-CT$^{EC536}$ and the formation of the catalytic site, consisting of α2 and the loop between α2 and α3 (Figures 2C, 3D and 7B), for tRNA cleavage. AlphaFold predicted that the N-terminal alpha helical region of *apo* CdiA-CT$^{EC536}$ might have alternative conformations: an extended long helix (A1) or a bent form with two helices (α1 and α 2) (Figure 3D, Supplementary Figure 5). In the CysK:CdiA-CT$^{EC536}$ ternary complex, the N-terminal region of CdiA-CT$^{EC536}$ adopts the bent conformation, stabilized by interactions between α2, α3, and α4. Thus, CysK provides a platform for CdiA-CT$^{EC536}$ to recognize and cleave the tRNA substrates.

Recently, it was shown that angiogenin (ANG), a secreted small RNaseA-type (125 amino acids) ribonuclease that cleaves the tRNA anticodon loop and promotes blood vessel formation (38–43), is activated by the ribosome (44). Although ANG reportedly cleaves the tRNA anticodon loop, enzymatic kinetic studies demonstrated that the tRNA cleavage efficiency is very low (38,45,46). In the recent study, it was shown that ANG binds to the ribosome A-site and changes its structure to an active form. Elongation factor eEF-1A delivers aminoacyl-tRNA (aa-tRNA) to the A-site, thereby allowing the tRNA anticodon loop to be cleaved by activated ANG in the ribosome A-site. Thus, the ribosome provides the platform for ANG to cleave the tRNA anticodon efficiently. The function of CysK in tRNA anticodon cleavage by the CysK:CdiA-CT$^{EC536}$ complex is analogous to that of the ribosome in

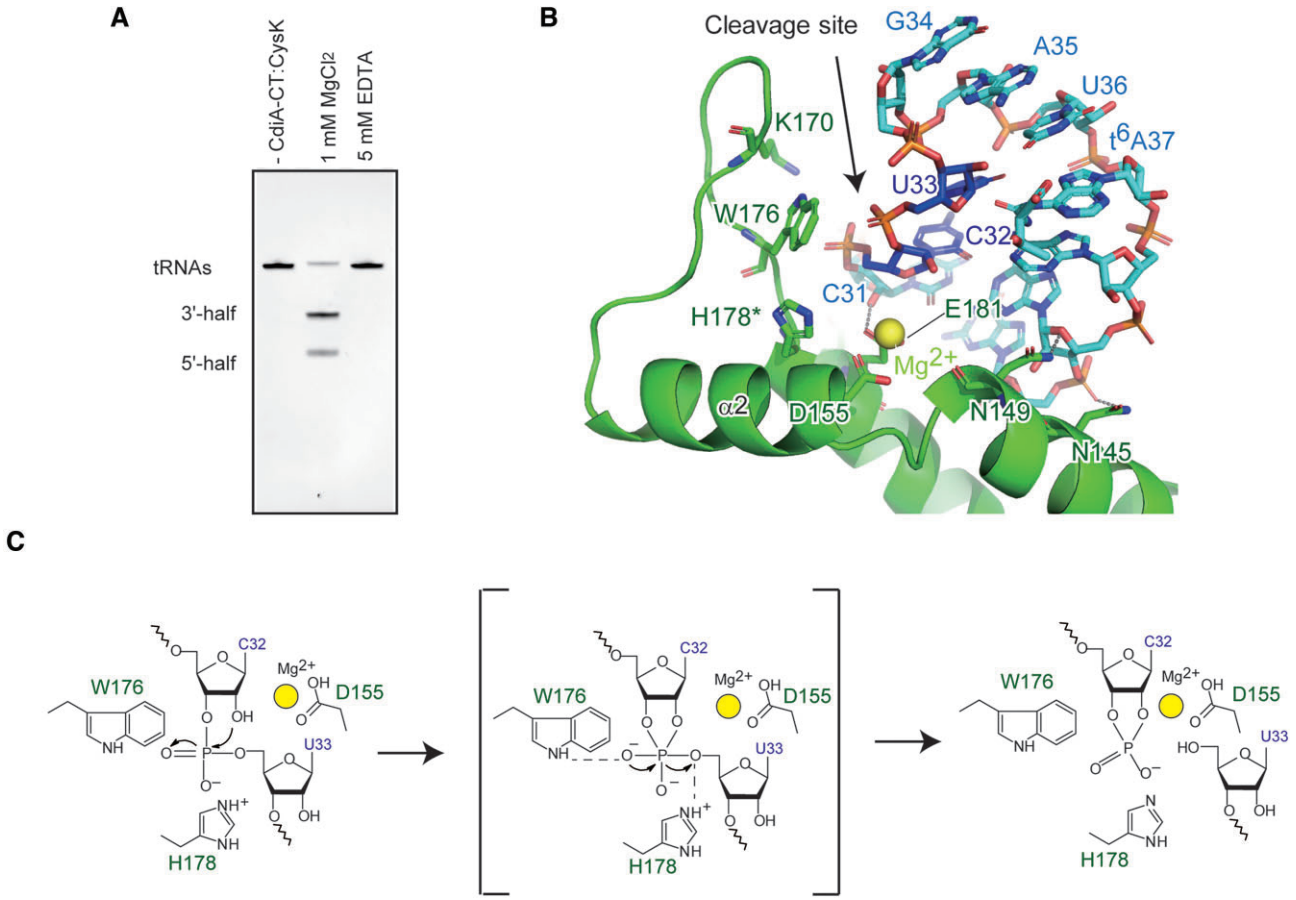


**Figure 7.** Possible metal-ion assisted catalytic mechanism of CdiA-CT$^{EC536}$. (**A**) tRNA cleavage by CysK:CdiA-CT$^{EC536}$ is $Mg^{2+}$-dependent. *E. coli* tRNA$^{Ile}$GCU (1 μM) was incubated with 0.5 μM CysK:CdiA-CT$^{EC536}$ in either the presence of 1 mM $MgCl_2$ or 5 mM EDTA at 37°C for 20 min. (**B**) Close-up view of the catalytic site of CdiA-CT$^{EC536}$ in complex with tRNA. The anticodon stem-loop of tRNA is represented by a cyan stick model. Nucleotides at positions 32 and 33 are colored blue. CdiA-CT$^{EC536}$ is colored green and the $Mg^{2+}$ ion is yellow. H178A was replaced with H178 (*) in the CdiA-CT$^{EC536}$ structure. (**C**) Possible metal-assisted catalytic mechanism of tRNA cleavage by CdiA-CT$^{EC536}$.

tRNA cleavage by ANG on ribosomes (Figure 8). CysK activates CdiA-CT$^{EC536}$, which then interacts with the bottom-half of the tRNA, recognizes the structures of the D stem-loop and anticodon stem-loop, thereby cleaves tRNA anticodon. *In vivo*, under normal physiological conditions, most tRNAs exist as aa-tRNAs (47), which form complexes with the translation elongation factors EF-Tu and −Ts. EF-Tu:GTP (PDB ID 1OB2) (48) or ET-Tu:GTP:Ts (PDB ID 4PC7) (49) binding to aa-tRNA and CdiA-CT$^{EC536}$ in CysK:CdiA-CT$^{EC536}$ binding to aa-tRNA are not mutually exclusive (Supplementary Figure 6). Thus, like ANG, CdiA-CT$^{EC536}$ targets aa-tRNAs and/or their complexes with translational elongation factors, rather than uncharged-tRNAs, *in vivo*. Other bacterial tRNase toxins, such as colicin E and colicin D, have intrinsic tRNase activities that cleave the anticodon loops of specific groups of tRNAs (50,51). For two decades, the exact mechanisms of tRNA recognition and cleavage by these toxins have not been well understood. Like CdiA-CT$^{EC536}$ and ANG, these toxins might also require some additional factors that act as platforms for tRNA recognition and cleavage by these toxins.

Analyses of tRNA cleavage upon expression of CdiA-CT$^{EC536}$ in *E. coli* showed that most tRNAs were cleaved to various extents by the action of CdiA-CT *in vivo* (Supplementary Figure 7). The anticodon-loop modifications of tRNAs would affect their cleavage by the CysK:CdiA-CT$^{EC536}$ complex. Under the conditions tested, tRNAs such as tRNA$^{Lys}$UUU, tRNAf$^{Met}$CAU, tRNA$^{Leu}$CAG, tRNA$^{Tyr}$GUA, tRNA$^{Trp}$CCA and tRNA$^{Gln}$CUG were not significantly cleaved *in vivo*. tRNAf$^{Met}$CAU, tRNA$^{Trp}$CCA, and tRNA$^{Gln}$CUG have either 2′-*O*-methyl cytidine (Cm) or uridine (Um) at position 32. The presence of Cm/Um at position 32 explains why these tRNAs cannot be cleaved by CdiA-CT$^{EC536}$, considering the possible catalytic mechanism (Figure 7C). The slight cleavage of tRNA$^{Gln}$CUG might be due to the hypomodification of U32 to Um32. tRNA$^{Lys}$UUU has mnm$^5$S$^2$U at the anticodon's first position. The modification would affect the structure of the anticodon loop and reduce the cleavage efficiency by CdiA-CT$^{EC536}$ (Supplementary Figure 7). In addition to modifications in the anticodon loop region, the structure of the variable loop (V-loop) would also affect tRNA cleavage by CdiA-CT$^{EC536}$. tRNA$^{Leu}$CAG and tRNA$^{Tyr}$GUA, together with tRNA$^{Ser}$GCU, are class-II tRNAs with longer V-loops. The D-loop structure of the class-II tRNAs would be different from that of class-I tRNAs, since the V-loop interacts with the D-loop. The longer variable loop might lead to the reduced affinity of class-II tRNAs toward CdiA-CT$^{EC536}$, thus reducing the efficiency of class-II tRNA cleavage by CdiA-CT$^{EC536}$.

CdiA-CT$^{EC536}$ utilizes a metal-ion-assisted mechanism for tRNA cleavage (Figure 7A). In the proposed catalytic model

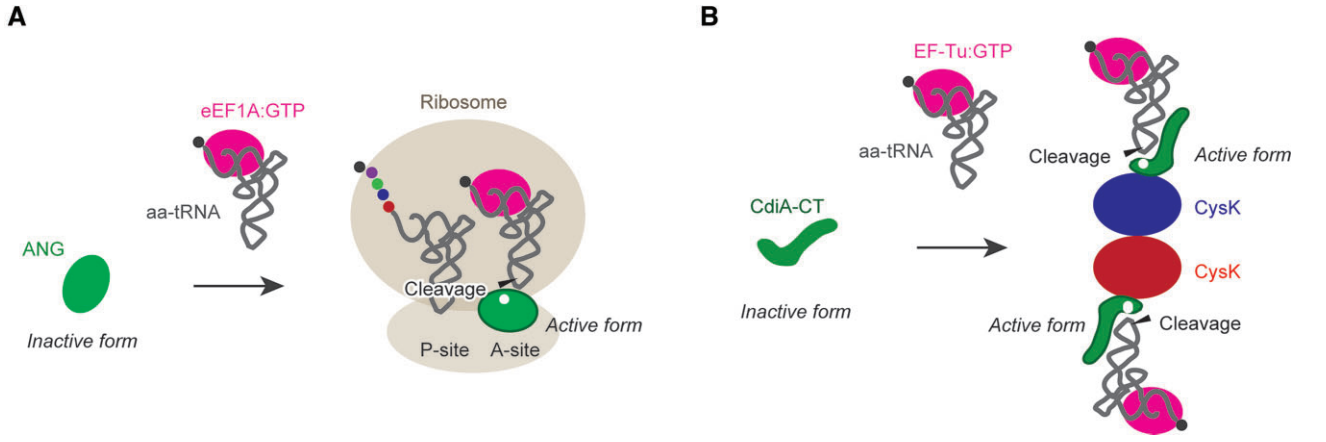


**Figure 8.** CysK activates CdiA-CT$^{EC536}$. The function of CysK in tRNA anticodon cleavage by the CysK:CdiA-CT$^{EC536}$ complex is analogous to that of the ribosome in tRNA cleavage by angiogenin (ANG) on ribosomes. (**A**) Activation of ANG on the A-site of ribosomes. eEF-1A delivers aminoacyl-tRNA (aa-tRNA) to the A-site, thereby allowing the tRNA anticodon loop to be cleaved by activated ANG within the ribosome A-site. (**B**) Activation of CdiA-CT$^{EC536}$ on CysK. Activated CdiA-CT$^{EC536}$on CysK interacts with the bottom-half of aa-tRNA or EF-Tu (GTP):aa-tRNA, recognizing the structures of the D stem-loop and anticodon stem-loop, thereby cleaving tRNA anticodon loop.

(Figure 7B,C), the hydroxide ion of a hydrated $Mg^{2+}$ ion, coordinated to D155, acts as a general base and deprotonates the 2′-hydroxyl group of the C32 ribose. The metal-assisted deprotonation of the 2′-hydroxyl group was previously suggested in RNA cleavage reactions by hammerhead ribozymes (52,53). H178 acts as a general acid and donates a proton to the 5′-leaving oxygen of C33. The functions of the hydroxide ion of a hydrated $Mg^{2+}$ ion, coordinated to D155, and H178 in CdiA-CT$^{EC536}$ correspond to those of the two histidine residues functioning as a general acid and base in RNase A (54).

In conclusion, the present study reveals the cryo-EM structure of the CysK:CdiA-CT$^{EC536}$:tRNA ternary complex, elucidating the tRNA recognition and cleavage mechanisms. The tRNA interacts solely with CdiA-CT$^{EC536}$, which uses its α-helices to clamp the D-stem and anticodon stem, thus positioning the anticodon loop in the active site. CysK stabilizes the CdiA-CT$^{EC536}$ structure, forming the catalytic site for tRNA cleavage upon tRNA binding to CdiA-CT$^{EC536}$, and thus activating CdiA-CT$^{EC536}$. This mechanism is conceptually analogous to the quite recently identified ribosome-mediated activation of the anticodon tRNase ANG (44), highlighting the utilization of other proteins as reaction platforms to facilitate efficient tRNA cleavage in the bacterial CDI system.

## Data availability

The atomic coordinates and cryo-EM maps of CysK:CdiA-CT$^{EC536}$:tRNA complex-A and −B have been deposited in the Protein Data Bank (PDB 8ZYC and 8ZYD), and the Electron Microscopy Data bank (EMD-60561and EMD-60562), respectively. The EM maps for the 2:2 CysK:CdiA-CT$^{EC536}$ and 2:1 CysK:CdiA-CT$^{EC536}$ complexes have been deposited in the Electron Microscopy Data bank (EMD-60564 and EMD-60563, respectively). The micrographs of CysK:CdiA-CT$^{EC536}$:tRNA have been deposited in the Electron Microscopy Public Image Archive ( EMPIAR-12146).

## Supplementary data

Supplementary Data are available at NAR Online.

## Acknowledgements

We thank staff of Cryo-electron Microscopy Facility at the University of Tokyo for technical assistance during data collection.

## Funding

Grants-in-Aid for Scientific Research (A) [23H00368, 18H03980, 26251009 to K.T.]; K.T. was also supported by grants from the Institute for Fermentation; Takeda Science Foundation; Naito Foundation; Kobayashi Foundation; the cryo-EM data collection was supported by Research Support Project for Life Science and Drug Discovery (Basis for Supporting Innovative Drug Discovery and Life Science Research (BINDS)) from AMED [JP23ama121002]. Funding for open access charge: Grant-in-Aid for Scientific Research (A) from JSPS [to K.T.].

## Conflict of interest statement

None declared.

## References

1. Aoki,S.K., Diner,E.J., de Roodenbeke,C.T., Burgess,B.R., Poole,S.J., Braaten,B.A., Jones,A.M., Webb,J.S., Hayes,C.S., Cotter,P.A., *et al.* (2010) A widespread family of polymorphic contact-dependent toxin delivery systems in bacteria. *Nature*, **468**, 439–442.
2. Ruhe,Z.C., Low,D.A. and Hayes,C.S. (2020) Polymorphic Toxins and Their Immunity Proteins: diversity, Evolution, and Mechanisms of Delivery. *Annu. Rev. Microbiol.*, **74**, 497–520.
3. Hayes,C.S., Koskiniemi,S., Ruhe,Z.C., Poole,S.J. and Low,D.A. (2014) Mechanisms and biological roles of contact-dependent growth inhibition systems. *Cold Spring Harb. Perspect. Med.*, **4**, a010025.
4. Ruhe,Z.C., Low,D.A. and Hayes,C.S. (2013) Bacterial contact-dependent growth inhibition. *Trends Microbiol.*, **21**, 230–237.
5. Willett,J.L., Ruhe,Z.C., Goulding,C.W., Low,D.A. and Hayes,C.S. (2015) Contact-dependent growth inhibition (CDI) and CdiB/CdiA two-partner secretion proteins. *J. Mol. Biol.*, **427**, 3754–3765.

6. Ruhe,Z.C., Subramanian,P., Song,K., Nguyen,J.Y., Stevens,T.A., Low,D.A., Jensen,G.J. and Hayes,C.S. (2018) Programmed secretion arrest and receptor-triggered toxin export during antibacterial contact-dependent growth inhibition. *Cell*, **175**, 921–933.
7. Ruhe,Z.C., Wallace,A.B., Low,D.A. and Hayes,C.S. (2013) Receptor polymorphism restricts contact-dependent growth inhibition to members of the same species. *mBio*, **4**, e00480-13.
8. Bartelli,N.L., Passanisi,V.J., Michalska,K., Song,K., Nhan,D.Q., Zhou,H., Cuthbert,B.J., Stols,L.M., Eschenfeldt,W.H., Wilson,N.G., *et al.* (2022) Proteolytic processing induces a conformational switch required for antibacterial toxin delivery. *Nat. Commun.*, **13**, 5078.
9. Aoki,S.K., Pamma,R., Hernday,A.D., Bickham,J.E., Braaten,B.A. and Low,D.A. (2005) Contact-dependent inhibition of growth in Escherichia coli. *Science*, **309**, 1245–1248.
10. Morse,R.P., Nikolakakis,K.C., Willett,J.L.E., Gerrick,E., Low,D.A., Hayes,C.S. and Goulding,C.W. (2012) Structural basis of toxicity and immunity in contact-dependent growth inhibition (CDI) systems. *Proc. Natl. Acad. Sci. U.S.A.*, **109**, 21480–21485.
11. Cuthbert,B.J., Hayes,C.S. and Goulding,C.W. (2022) Functional and structural diversity of bacterial contact-dependent growth inhibition effectors. *Front. Mol. Biosci.*, **9**, 866854.
12. Diner,E.J., Beck,C.M., Webb,J.S., Low,D.A. and Hayes,C.S. (2012) Identification of a target cell permissive factor required for contact-dependent growth inhibition (CDI). *Genes Dev.*, **26**, 515–525.
13. Johnson,P.M., Beck,C.M., Morse,R.P., Garza-Sánchez,F., Low,D.A., Hayes,C.S. and Goulding,C.W. (2016) Unraveling the essential role of CysK in CDI toxin activation. *Proc. Natl. Acad. Sci. U.S.A.*, **113**, 9792–9797.
14. Kaundal,S., Uttam,M. and Thakur,K.G. (2016) Dual role of a biosynthetic enzyme, CysK, in contact dependent growth inhibition in bacteria. *PLoS One*, **11**, e0159844.
15. Benoni,R., Beck,C.M., Garza-Sánchez,F., Bettati,S., Mozzarelli,A., Hayes,C.S. and Campanini,B. (2017) Activation of an anti-bacterial toxin by the biosynthetic enzyme CysK: mechanism of binding, interaction specificity and competition with cysteine synthase. *Sci. Rep.*, **7**, 8817.
16. Michalska,K., Gucinski,G.C., Garza-Sanchez,F., Johnson,P.M., Stols,L.M., Eschenfeldt,W.H., Babnigg,G., Low,D.A., Goulding,C.W., Joachimiak,A., *et al.* (2017) Structure of a novel antibacterial toxin that exploits elongation factor Tu to cleave specific transfer RNAs. *Nucleic Acids Res.*, **45**, 10306–10320.
17. Jones,A.M., Garza-Sánchez,F., So,J., Hayes,C.S. and Low,D.A. (2017) Activation of contact-dependent antibacterial tRNase toxins by translation elongation factors. *Proc. Natl. Acad. Sci. U.S.A.*, **114**, E1951–E1957.
18. Gucinski,G.C., Michalska,K., Garza-Sánchez,F., Eschenfeldt,W.H., Stols,L., Nguyen,J.Y., Goulding,C.W., Joachimiak,A. and Hayes,C.S. (2019) Convergent evolution of the Barnase/EndoU/Colicin/RelE (BECR) fold in antibacterial tRNase toxins. *Structure*, **27**, 1660–1674.
19. Huang,R.H. (2019) Ribotoxins kill cells by chopping off the head of tRNAs. *Structure*, **27**, 1613–1614.
20. Wang,J., Yashiro,Y., Sakaguchi,Y., Suzuki,T. and Tomita,K. (2022) Mechanistic insights into tRNA cleavage by a contact-dependent growth inhibitor protein and translation factors. *Nucleic Acids Res.*, **50**, 4713–4731.
21. Yashiro,Y., Zhang,C., Sakaguchi,Y., Suzuki,T. and Tomita,K. (2021) Molecular basis of glycyl-tRNA(Gly) acetylation by TacT from Salmonella Typhimurium. *Cell Rep.*, **37**, 110130.
22. Zhang,C., Yashiro,Y., Sakaguchi,Y., Suzuki,T. and Tomita,K. (2020) Substrate specificities of Escherichia coli ItaT that acetylates aminoacyl-tRNAs. *Nucleic Acids Res.*, **48**, 7532–7544.
23. Yashiro,Y., Sakaguchi,Y., Suzuki,T. and Tomita,K. (2020) Mechanism of aminoacyl-tRNA acetylation by an aminoacyl-tRNA acetyltransferase AtaT from enterohemorrhagic E. coli. *Nat. Commun.*, **11**, 5438.
24. Guillon,J.M., Meinnel,T., Mechulam,Y., Lazennec,C., Blanquet,S. and Fayat,G. (1992) Nucleotides of tRNA governing the specificity of Escherichia coli methionyl-tRNA(fMet) formyltransferase. *J. Mol. Biol.*, **224**, 359–367.
25. Meinnel,T. and Blanquet,S. (1995) Maturation of pre-tRNA(fMet) by Escherichia coli RNase P is specified by a guanosine of the 5′-flanking sequence. *J. Biol. Chem.*, **270**, 15908–15914.
26. Yashiro,Y., Yamashita,S. and Tomita,K. (2019) Crystal structure of the Enterohemorrhagic Escherichia coli AtaT-AtaR toxin-antitoxin complex. *Structure*, **27**, 476–484.
27. Punjani,A., Rubinstein,J.L., Fleet,D.J. and Brubaker,M.A. (2017) cryoSPARC: algorithms for rapid unsupervised cryo-EM structure determination. *Nat. Methods*, **14**, 290–296.
28. Rubinstein,J.L. and Brubaker,M.A. (2015) Alignment of cryo-EM movies of individual particles by optimization of image translations. *J. Struct. Biol.*, **192**, 188–195.
29. Punjani,A., Zhang,H. and Fleet,D.J. (2020) Non-uniform refinement: adaptive regularization improves single-particle cryo-EM reconstruction. *Nat. Methods*, **17**, 1214–1221.
30. Zivanov,J., Nakane,T. and Scheres,S.H.W. (2020) Estimation of high-order aberrations and anisotropic magnification from cryo-EM data sets in RELION-3.1. *IUCrJ*, **7**, 253–267.
31. Sanchez-Garcia,R., Gomez-Blanco,J., Cuervo,A., Carazo,J.M., Sorzano,C.O.S. and Vargas,J. (2021) DeepEMhancer: a deep learning solution for cryo-EM volume post-processing. *Commun. Biol.*, **4**, 874.
32. Meng,E.C., Goddard,T.D., Pettersen,E.F., Couch,G.S., Pearson,Z.J., Morris,J.H. and Ferrin,T.E. (2023) UCSF ChimeraX: tools for structure building and analysis. *Protein Sci.*, **32**, e4792.
33. Afonine,P.V., Grosse-Kunstleve,R.W., Echols,N., Headd,J.J., Moriarty,N.W., Mustyakimov,M., Terwilliger,T.C., Urzhumtsev,A., Zwart,P.H. and Adams,P.D. (2012) Towards automated crystallographic structure refinement with phenix.refine. *Acta. Crystallogr. D Biol. Crystallogr.*, **68**, 352–367.
34. Liebschner,D., Afonine,P.V., Baker,M.L., Bunkóczi,G., Chen,V.B., Croll,T.I., Hintze,B., Hung,L.W., Jain,S., McCoy,A.J., *et al.* (2019) Macromolecular structure determination using X-rays, neutrons and electrons: recent developments in Phenix. *Acta Crystallogr. D Struct. Biol.*, **75**, 861–877.
35. Emsley,P., Lohkamp,B., Scott,W.G. and Cowtan,K. (2010) Features and development of Coot. *Acta. Crystallogr. D Biol. Crystallogr.*, **66**, 486–501.
36. Willett,J.L., Gucinski,G.C., Fatherree,J.P., Low,D.A. and Hayes,C.S. (2015) Contact-dependent growth inhibition toxins exploit multiple independent cell-entry pathways. *Proc. Natl. Acad. Sci. U.S.A.*, **112**, 11341–11346.
37. Jumper,J., Evans,R., Pritzel,A., Green,T., Figurnov,M., Ronneberger,O., Tunyasuvunakool,K., Bates,R., Žídek,A., Potapenko,A., *et al.* (2021) Highly accurate protein structure prediction with AlphaFold. *Nature*, **596**, 583–589.
38. Shapiro,R., Riordan,J.F. and Vallee,B.L. (1986) Characteristic ribonucleolytic activity of human angiogenin. *Biochemistry*, **25**, 3527–3532.
39. Fett,J.W., Strydom,D.J., Lobb,R.R., Alderman,E.M., Bethune,J.L., Riordan,J.F. and Vallee,B.L. (1985) Isolation and characterization of angiogenin, an angiogenic protein from human carcinoma cells. *Biochemistry*, **24**, 5480–5486.
40. Saxena,S.K., Rybak,S.M., Davey,R.T. Jr, Youle,R.J. and Ackerman,E.J. (1992) Angiogenin is a cytotoxic, tRNA-specific ribonuclease in the RNase A superfamily. *J. Biol. Chem.*, **267**, 21982–21986.
41. Yamasaki,S., Ivanov,P., Hu,G.F. and Anderson,P. (2009) Angiogenin cleaves tRNA and promotes stress-induced translational repression. *J. Cell Biol.*, **185**, 35–42.
42. Fu,H., Feng,J., Liu,Q., Sun,F., Tie,Y., Zhu,J., Xing,R., Sun,Z. and Zheng,X. (2009) Stress induces tRNA cleavage by angiogenin in mammalian cells. *FEBS Lett.*, **583**, 437–442.

43. Ivanov,P., Emara,M.M., Villen,J., Gygi,S.P. and Anderson,P. (2011) Angiogenin-induced tRNA fragments inhibit translation initiation. *Mol. Cell*, **43**, 613–623.
44. Loveland,A.B., Koh,C.S., Ganesan,R., Jacobson,A. and Korostelev,A.A. (2024) Structural mechanism of angiogenin activation by the ribosome. *Nature*, **630**, 769–776.
45. Russo,N., Shapiro,R., Acharya,K.R., Riordan,J.F. and Vallee,B.L. (1994) Role of glutamine-117 in the ribonucleolytic activity of human angiogenin. *Proc. Natl. Acad. Sci. U.S.A.*, **91**, 2920–2924.
46. Jardine,A.M., Leonidas,D.D., Jenkins,J.L., Park,C., Raines,R.T., Acharya,K.R. and Shapiro,R. (2001) Cleavage of 3′,5′-pyrophosphate-linked dinucleotides by ribonuclease A and angiogenin. *Biochemistry*, **40**, 10262–10272.
47. Evans,M.E., Clark,W.C., Zheng,G. and Pan,T. (2017) Determination of tRNA aminoacylation levels by high-throughput sequencing. *Nucleic Acids Res.*, **45**, e133.
48. Nissen,P., Kjeldgaard,M., Thirup,S., Polekhina,G., Reshetnikova,L., Clark,B.F. and Nyborg,J. (1995) Crystal structure of the ternary complex of Phe-tRNAPhe, EF-Tu, and a GTP analog. *Science*, **270**, 1464–1472.
49. Thirup,S.S., Van,L.B., Nielsen,T.K. and Knudsen,C.R. (2015) Structural outline of the detailed mechanism for elongation factor Ts-mediated guanine nucleotide exchange on elongation factor Tu. *J. Struct. Biol.*, **191**, 10–21.
50. Tomita,K., Ogawa,T., Uozumi,T., Watanabe,K. and Masaki,H. (2000) A cytotoxic ribonuclease which specifically cleaves four isoaccepting arginine tRNAs at their anticodon loops. *Proc. Natl. Acad. Sci. U.S.A.*, **97**, 8278–8283.
51. Ogawa,T., Tomita,K., Ueda,T., Watanabe,K., Uozumi,T. and Masaki,H. (1999) A cytotoxic ribonuclease targeting specific transfer RNA anticodons. *Science*, **283**, 2097–2100.
52. Hanna,R. and Doudna,J.A. (2000) Metal ions in ribozyme folding and catalysis. *Curr. Opin. Chem. Biol.*, **4**, 166–170.
53. Wang,S., Karbstein,K., Peracchi,A., Beigelman,L. and Herschlag,D. (1999) Identification of the hammerhead ribozyme metal ion binding site responsible for rescue of the deleterious effect of a cleavage site phosphorothioate. *Biochemistry*, **38**, 14363–14378.
54. Thompson,J.E. and Raines,R.T. (1994) Value of general acid-base catalysis to ribonuclease A. *J. Am. Chem. Soc.*, **116**, 5467–5468.
55. Sprinzl,M., Grueter,F., Spelzhaus,A. and Gauss,D.H. (1980) Compilation of tRNA sequences. *Nucleic Acids Res.*, **8**, r1–r22.




**Received:** July 2, 2024. **Revised:** August 9, 2024. **Editorial Decision:** August 11, 2024. **Accepted:** August 14, 2024